Accepted Manuscript

Design, synthesis, in-silico and biological evaluation of novel chalcone-*O*-carbamate derivatives as multifunctional agents for the treatment of Alzheimer's disease

Zhipei Sang, Keren Wang, Jian Shi, Wenmin Liu, Zhenghuai Tan

PII: S0223-5234(19)30551-3

DOI: https://doi.org/10.1016/j.ejmech.2019.06.026

Reference: EJMECH 11429

To appear in: *European Journal of Medicinal Chemistry*

Received Date: 27 April 2019

Revised Date: 25 May 2019

Accepted Date: 9 June 2019

Please cite this article as: Z. Sang, K. Wang, J. Shi, W. Liu, Z. Tan, Design, synthesis, in-silico and biological evaluation of novel chalcone-*O*-carbamate derivatives as multifunctional agents for the treatment of Alzheimer's disease, *European Journal of Medicinal Chemistry* (2019), doi: https://doi.org/10.1016/j.ejmech.2019.06.026.

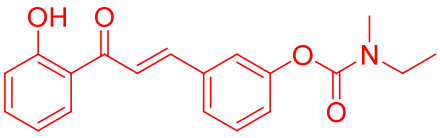

5b

Reversible comprtition BChE inhibitor, IC_{50} = 3.1μM;
Selective MAO-B inhibitor, IC_{50} = 1.3μM;
ORAC = 1.3eq; Neuroprotective agent; Selective metal chelator;
Inhibition of self-induced Aβ aggregation: 63.9%
Inhibition of Cu^{2+}-induced Aβ aggregation: 78.3%
Disaggregation of Cu^{2+}-induced Aβ aggregation: 83.1%
Could cross PAMPA-BBB and conformed to the Lipinski's rule
Presented precognitive effect

Design, synthesis, in-silico and biological evaluation of novel chalcone-*O*-carbamate derivatives as multifunctional agents for the treatment of Alzheimer's disease

Zhipei Sang[a,#*], *Keren Wang*[a,#], *Jian Shi*[a], *Wenmin Liu*[a,*], *Zhenghuai Tan*[c,*].

[a] *College of Chemistry and Pharmaceutical Engineering, Nanyang Normal University, Nanyang, 473061, China*

[b] *Institute of Traditional Chinese Medicine Pharmacology and Toxicology, Sichuan Academy of Chinese Medicine Sciences, Chengdu, 610041, China*

Abbreviations: AD, Alzheimer's disease; FDA, Food and Drug Administration; AChEs acetylcholinesterase inhibitors; A*β*, *β*-amyloid; MTDLs, multitarget-directed ligands; ACh, acetylcholine; ROS, reactive oxygen species; MAO, monoamine oxidase; BChE, butylcholinesterase; 4-DMAP, 4-dimethylaminopyridine; PDB, Protein Data Bank; ORAC-FL, Oxygen Radicals Absorbance Capacity by Fluorescence; ThT, thioflavin T; TEM, transmission electron microscopy; MTT, 3-(4,5-dimethylthiazol-2-yl)-2,5-diphenyltetrazolium; PAMPA-BBB, parallel artificial membrane permeation assay of the blood−brain barrier; TPSA, topological polar surface area; TLC, thin-layer chromatography; HPLC, high-performance liquid chromatography; PBL, procine brain lipid.

**Corresponding Author*.

E-mail: sangzhipei@126.com (Zhipei Sang)

E-mail: liuwm1969@163.com (Wenmin Liu)

E-mail: tanzhh616@163.com (Zhenghuai Tan)

Abstract

To discover multifunctional agents for the treatment of Alzheimer's disease (AD), a series of chalcone-*O*-carbamate derivatives was designed and synthesized based on the multitarget-directed ligands strategy. The *in vitro* biological activities were evaluated including AChE/BChE inhibition, MAO-A/MAO-B inhibition, antioxidant activities, $A\beta_{1-42}$ aggregation inhibition, metal-chelating properties and neuroprotective effects against H_2O_2-induced PC12 cell injury. The results showed compounds **5b** and **5h** indicated highly selective BChE inhibitory activity with IC_{50} values of 3.1 μM and 1.2 μM, respectively and showed highly selective MAO-B inhibitory potency with IC_{50} values of 1.3 μM and 3.7 μM, respectively. In addition, compounds **5b** and **5h** could inhibit self-induced $A\beta_{1-42}$ aggregation with 63.9% and 53.1% inhibition percent rate, respectively. Particularly, compound **5b** was a potent antioxidant agent and neuroprotectant, as well as a selective metal chelator by chelating Cu^{2+} and Al^{3+}. Moreover, compound **5b** could inhibit and disaggregate Cu^{2+}-induced $A\beta_{1-42}$ aggregation, which was further supported by the TEM images. Furthermore, compounds **5b** and **5h** could cross the blood-brain barrier (BBB) *in vitro* and conformed to the Lipinski's rule of five. Finally, the *in vivo* assay exhibited that compound **5b** could improve scopolamine-induced cognitive impairment. Taken together, these results revealed that compound **5b** might be a potential multifunctional agent for the treatment of AD, and deserved to do further structure optimization.

Keywords: Alzheimer's disease; Chalcone-*O*-carbamate derivatives; Butylcholinesterase inhibitors; Monoamine oxidase B inhibitor; Antioxidant agents; Neuroprotective effect; A*β* aggregation inhibitors; Biometals chelator; Precognitive effect

1. Introduction

Alzheimer's disease (AD) is an age-related neurodegenerative disease featuring progressive memory loss, language skills decline, and other cognitive impairments [1]. Nearly 36 million people are affected by Alzheimer's disease today, and three times more are projected to be affected in 2050 [2]. Currently, the clinical drugs approved by FDA for AD patients are focused on acetylcholinesterase inhibitors (AChEs) such as donepezil, galantamine and rivastigmine. Although these single target drugs could temporarily delay the progression of cognitive decline in AD, their effects are modest. In addition, AChEIs produce several undesirable side effects, such as gastrointestinal disturbances, bradycardia, and excessive salivation, which are associated with peripheral cholinergic receptors [3]. Up to now, the etiology of AD is not fully understood, but several factor, such as cholinergic dysfunction, amyloid-β (Aβ) deposits, tau protein aggregation, oxidative stress and metal ion disorder are considered to serve as important roles in the pathophysiology of AD [4]. Therefore, an appropriate strategy to achieve better therapeutic efficacy for AD is proposed by development of multitarget-directed ligands (MTDLs) that can simultaneously modulate different targets or mechanisms involved in the neurodegenerative AD cascade [5-7].

The classical "cholinergic hypothesis" has been widely accepted by researchers and many efforts have been made to seek selective AChE inhibitors for the treatment of AD [8-10]. The recent studies show that AChE is selectively responsible for hydrolyzing neurotransmitter acetylcholine (ACh) in the healthy brain and the early stages of AD, while BChE, possessing wider substrate specific than AChE, acts as the major ACh degrading enzyme in AD progression [11]. Additionally, in the brain of healthy human, both AChE and BChE are found in the ration of 4:1. However, AChE activity in the AD brain decline progressively by up to 45%, leading to the loss of neurons and axons, while BChE activity enhanced by up to two-fold in cortex and hippocampus [12]. This suggests that BChE takes over the hydrolysis of ACh in AD brain. Moreover, selective BChE inhibition might circumvent the classical cholinergic toxicity that is a common side effect of AChE inhibition [13]. Therefore, selective

BChE inhibitors are proposed strategy for the treatment of AD, especially the advanced stages of AD.

According to the "amyloid hypothesis", the production and accumulation of oligomeric aggregates of Aβ are thought to initiate the pathogenic cascade, ultimately leading to neuronal loss and dementia, which are considered as a central event in the pathogenesis of AD [14, 15]. In addition, Aβ can efficiently generate reactive oxygen species (ROS) in the presence of some transition metals. Antioxidant enzymes have been observed to be increased in AD brain regions and oxidative damage is also present in the brain of AD patients, damaging biological macromolecules including proteins, lipids and nucleic acids [16-18]. In addition, redox-active metal ions like Cu^{2+}, Zn^{2+}, Al^{3+} and Fe^{2+} contribute to the production of ROS, which promotes oxidative stress, leading to AD pathogenesis [19, 20]. Therefore, antioxidants and modulation of such biometals in the brain have been considered as a potential therapeutic strategy to treat AD.

Monoamine oxidase (MAO) is a FAD-dependent enzyme, responsible for oxidative deamination of amine neurotransmitters, serves as an important target for the treatment of specific features of AD. MAO exists as two distinct enzymatic isoforms, MAO-A and MAO-B. Selective MAO-A inhibitors are used in the treatment of depression, while selective MAO-B inhibitors are useful in the treatment of AD because an increased level of MAO-B has been detected in the brain of AD patients [21-23]. Therefore, selective MAO-B inhibitors might be another way against AD.

Chalcone (1,3-diary-2-propen-1-one) is a simple chemical scaffold of many naturally occurring compounds and has a widespread distribution in vegetables, fruits, teas, and other plants [24]. Chalcone compounds are prominent secondary-metabolite precursors of flavonoids and isoflavonoids, and also presented multiple biological activities including anti-inflammatory, MAO-B inhibition, radical-scavenging and neuroprotective properties, which would contribute to the treatment of AD [25]. But, the lack of ChEs inhibition and metal chelation limited its application in AD therapy. Rivastigmine is a unique cholinesterase inhibitor with both AChE and

butyrylcholinesterase (BChE) inhibitory activity and is also available as transdermal patch that has been approved by FDA for the treatment of mild, moderate, and severe AD [26]. It has been shown that the carbamate moiety in rivastigmine is the cholinesterase-inhibitory pharmacophore and that it can covalently bind to the enzyme and remains attached until it is slowly removed by hydrolysis [27]. In addition, in our previous work, the derivatives possessing adjacent hydroxyl group and carbonyl group could be selective metal chelators [28-30]. Therefore, we plan to use the MTDLs strategy to fuse chalcone, rivastigmine and metal chelation fragment and create a series of chalcone-*O*-carbamate derivatives (**Figure 1**), hoping these compounds possess complementary multi-functional activities.

<Insert **Figure 1**>

In this work, a series of chalcone-*O*-carbamate derivatives was designed based on MTDLs. These target compounds were synthesized and evaluated by AChE/BChE inhibition, antioxidant activity, MAO-A/MAO-B inhibition, A$\beta_{1\text{-}42}$ aggregation inhibition and disaggregation, biometals chelation properties, neuroprotective effect and the ability of cross blood-brain barrier *in vitro*. Further, the optimized molecule was evaluated *in vivo* assay. Moreover, docking studies were also used to provide rational explanation for their biological activities.

2. Results and discussion

2.1. Chemistry

The synthetic route of target compounds **5a~5l** were depicted in **Scheme 1**, 2-hydroxy acetophenone **1** as starting material was treated with 3-hydroxybenzaldehyde **2** in alcoholic 50% KOH solution to obtain the key intermediate chalcone **3**. Finally, compound **3** was treated with excessive amounts of *N*,*N*-disubstituted carbamoyl chlorides (**4a-4f**) in the presence of anhydrous K_2CO_3 and a catalytic amount 4-dimethylaminopyridine (4-DMAP) in CH_3CN at 60–65°C to afford the target compounds **5a-5l**. Their structures were confirmed by ^{1}H NMR, ^{13}C NMR and HR–MS spectroscopy.

<Insert **Scheme 1**>

2.2. Pharmacology

2.2.1. eeAChE and eqBChE Inhibition. The inhibition activity towards *ee*AChE and *eq*BChE for the target compounds **5a-5l** were evaluated using modified Ellman assay [31]. The parental compound **3** and positive compound rivastigmine and donepezil were also tested as control purpose. The IC_{50} values for AChE and BChE inhibition were summarized in **Table 1**. The results revealed that introduction of carbamate fragment significantly increased *eq*BChE inhibitory activity with IC_{50} values ranging from 56.2 μM to 1.2 μM, particularly, compounds **5h**, **5i** and **5l** indicated excellent eqBChE inhibitory activity compared with positive compound rivastigmine (*eq*BChE, IC_{50} = 1.3 μM), which was consistent with our design strategy. In addition, in **Table 1** almost all the target compounds were selective BChE inhibitors because they exhibited weak eeAChE inhibitory potency, except compounds **5e** and **5k** with the carbamate moieties containing *N*,*N*-diphenylamine group.

The carbamate substitution significantly affected eqBChE inhibitory activity. When the carbamate moieties at the 3 position of chalcone, target compound **5a** with *N*,*N*-dimethylamine group showed good eqBChE inhibitory activity with IC_{50} value was 2.51 μM, changing *N*,*N*-dimethylamine group of **5a** with *N*-ethyl-*N*-methylamine and *N*-methoxymethylamine to obtain **5b** and **5c**, respectively, the *eq*BChE inhibitory activity showed slightly decreased with IC_{50} value was 3.1 μM and 3.2μM, respectively. Replacing *N*,*N*-dimethylamine group of **5a** with *N*,*N*-diethylamine to get **5d**, the *eq*BChE inhibitory activity decreased to 4.8 μM, and then compound **5f** with morpholine group was obtained by means of ringclosure from *N*,*N*-dimethylamine group, **5f** displayed good *eq*BChE inhibitory activity with IC_{50} value was 5.1 μM. While, replacing *N*,*N*-dimethylamine group of **5a** with *N*,*N*-diphenylamine group to get **5e**, the eqBChE sharply decreased to 56.2 μM. The phenomenon revealed that the aliphatic series *N*,*N*-disubstituted carbamoyl contributed to the *eq*BChE inhibitory activity, while the aromatic *N*,*N*-disubstituted carbamoyl resulted in negative effect on *eq*BChE inhibitory potency.

Furthermore, the carbamate moieties at both 2’ and 3 position of chalcone also

had significantly effects on *eq*BChE inhibitory activity. Generally, disubstituted carbamate derivatives exhibited better *eq*BChE inhibitory activities that that of monosubstituted carbamate derivatives, such as **5b** < **5h**, **5c** < **5i**, **5d** < **5j**, **5e** < **5k** and **5f** < **5l**. Moreover, for the disubstituted carbamate derivatives, the potencies to inhibit *eq*BChE were in the order *N*-ethyl-*N*-methylamine (**5h**) > *N*-methoxymethylamine (**5i**) > morpholine (**5l**) > *N*,*N*-diethylamine (**5j**) > *N*,*N*-dimethylamine (**5g**) > *N*,*N*-diphenylamine (**5k**). The results observed revealed that carbamate moieties containing aliphatic amine groups and cyclic amine contributed to the *eq*BChE inhibitory activities, but the arylamine produced an adverse effect on *eq*BChE inhibitory activity. As for the *ee*AChE inhibition, the carbamate moieties did not show significant effect on AChE inhibitory activity. Therefore, the target compounds were promising selective *eq*BChE inhibitors, and compounds **5b** and **5h** were selected to further study.

<Insert **Table 1**>

*2.2.2 EqBChE reversibility of inhibition by **5b** and **5h**.* To further test the *eq*BChE reversibility inhibition by **5b** and **5h**, the recovery of *eq*BChE inhibitor inhibition after dilution (**Figure 2A**), with time monitoring (**Figure 2B**) were performed [32, 33]. As shown in **Figure 2A**, compared to controls, the 0.1 × IC_{50} of standard donepezil increased *eq*BChE activity to 8.8%, that is an indication of possible slow, partial recovery of the *eq*BChE from donepezil. While the 0.1 × IC_{50} of standard rivastigmine increased *eq*BChE activity to -2.9%, implying an indication of possible no recovery of the *eq*BChE from rivastigmie. In addition, under the same condition, the 0.1 × IC_{50} of compounds **5b** and **5h** increased *eq*BChE activity to 0.7% and 1.0%, respectively, showing on recovery of the *eq*BChE, as similarly with rivastigmine. Furthermore, as shown in **Figure 2B**, the *eq*BChE activity restored to 103.9% with 0.1× IC_{50} donepezil at 120 min, the *eq*BChE activity of 0.1× IC_{50} rivastigmine gradually increased to 71.6% at 120 min. As expected, and the *eq*BChE activity of 0.1× IC_{50} compounds **5b** and **5h** added up to 75.1% and 70.9%, respectively, at 120 min, like rivastigmine. Therefore, the observed results indicated that compounds **5b** and **5h** would be pseudo reversible inhibitors of BChE.

<Insert **Figure 2**>

*2.2.3 Enzyme kinetic of compound **5b***. Compound **5b** was selected to further assess kinetic study for testing the inhibitory mechanism of BChE [34]. As shown in **Figure 2**, graphical analysis showed both increasing slopes (decreased V_{max}) and intercepts at Y axe. It implied that compound **5b** was a reversible competitive inhibitor, and **5b** could compete with substrate BCh, binding with the active site of BChE.

<Insert **Figure 3**>

*2.2.4 Molecular modeling studies of **5b** and **5h***. The further computational study was performed to explore possible binding mechanism of AChE and BChE for compounds **5b** and **5h** using the docking program, AutoDock 4.2 package with Discovery Studio 2.5, based on the X-ray crystal structure of BChE (PDB code: 4tpk) and AChE (PDB code: 1EVE) [28, 35]. The results indicated that **5b** bind with BChE via multiple sites **(Figure 4)**. The hydroxyl group and carbonyl group of **5b** formed one intramolecular hydrogen bonding, and the hydroxyl group and the carbonyl group interacted with key amino acid Trp82 and important amino acid Gly121 via intermolecular hydrogen bonding, respectively. In addition, the benzene ring of chalcone skeleton interacted with key amino acid Trp82 via two π-π interactions, contributing to the BChE inhibitory activity. Meanwhile, hydrophobic interactions could be observed between the ligand and Trp82, Asp70, Ala328, Thr120, Gly116, His438. Furthermore, compound **5h** was also observed multiple interactions with BChE **(Figure 5)**, the two benzene rings of chalcone skeleton simultaneously formed π-π interactions with key amino acid Trp82 and important amine acid Tyr332, respectively. The carbonyl group of chalcone skeleton interacted with important amine acid Tyr332 via intermolecular hydrogen bonding, moreover, the oxygen atom of *O*-carbamate moiety could interact with key Thr120 through intermolecular hydrogen bonding. Besides, there were some hydrophobic interactions were observed between the ligand and Trp82, Asp70, Ala328, Thr120, Gly116, His438, Tyr332. The multiple interactions observed between ligands (**5b** and **5h**) and BChE provided reasonable explanation for their potent BChE inhibitory activity.

<Insert **Figure 4**>

<Insert **Figure 5**>

On the other hands, the possible binding mechanism of AChE for compounds **5b** and **5h** was also explored. In the **5b**-AChE complex (**Figure 6A**), there were two characteristic intermolecular hydrogen bonding were observed between ligand and amine acid. While, in the **5h**-AChE complex (**Figure 6B**), only one characteristic interaction was found between the Phe288 and the carbonyl group of **5h**. Therefore, the limited characteristic interaction explained the weak AChE inhibitory activity for compounds **5b** and **5h**, and further exhibited that compounds **5b** and **5h** were promising selective BChE inhibitors.

<Insert **Figure 6**>

2.2.5 Antioxidant Activity in Vitro. Oxygen Radicals Absorbance Capacity by Fluorescence (ORAC-FL) method was used to test the antioxidant activity of target compounds **5a-5l** [29]. The vitamin E analogue Trolox was used as a standard, and the parent compound **3** was also tested as control purpose. The screening data were listed in **Table 1**, all the compounds showed exhibited potent antioxidant activity with ORAC-FL values of 0.31−1.3 Trolox equivalents (*eq*), but presented lower antioxidant potency than parent compound **3** (2.6 *eq* Trolox). In addition, monosubstituted carbamate derivatives (**5a-5f**) showed better antioxidant activity than that of disubstituted carbamate derivatives (**5g-5l**). As expected, the introduction of carbamate moieties in the chalcone nucleus decreased the radical capture capacity, while the different tertiary amine unit on the carbamate fragment produced little influence on the radical capture capacity. The results observed revealed that the hydroxyl group played crucial role in the antioxidant activity, and the compound **5b** (1.3 *eq*) possessing mono-*N*-ethyl-*N*-methyl carbamate showed better antioxidant activity than that of **5h** (0.35 *eq*) with disubstituted carbamate.

2.2.6 huMAO-A and huMAO-B inhibition. The MAO-A and MAO-B (from recombinant human enzyme) inhibitory potency of **5a-5l** were determined using fluorescence assay [36, 37]. Iproniazid and rasagiline were tested as referenced compounds. The parent compound **3** was also assessed as control purpose, which was a selective huMAO-B inhibitor with IC_{50} value was 1.1 μM. The screening data in

Table 2 revealed that all the target compounds showed good huMAO-B inhibitory potency, and weak huMAO-A inhibitory activity compared with compound **3**. So, the synthetic target compounds were selective huMAO-B inhibitors, which was consistent with our design strategy. In addition, introduction of carbamate fragment weakened MAO-B inhibitory activities, and the tertiary amine unit in carbamate moieties showed potent effect on huMAO-B inhibitory activities. Generally, the target compounds **5a-5d** possessing aliphatic amine displayed better huMAO-B inhibitory activity than the compounds **5e** and **5f** with cyclamine and arylamine, respectively. The huMAO-B inhibitory potency were in order *N*,*N*-dimethylamine (**5g**) > *N*-ethyl-*N*-methylamine (**5b**) > *N*,*N*-diethylamine (**5j**) >*N*-methoxymethylamine (**5i**) > morpholine (**5l**) > *N*,*N*-diphenylamine (**5k**). Moreover, the compounds (**5g-5l**) with disubstituted carbamate fragment indicated lower *hu*MAO-B inhibitory activity than the compounds (**5a-5f**) with monosubstituted carbamate. According to the results observed, compound **5a** exhibited the best *hu*MAO-B inhibitory activity with IC_{50} value was 0.8 μM, and the representative compounds **5b** and **5h** were potent selective huMAO-B inhibitors with IC_{50} values were 1.3 μM and 3.7 μM, respectively.

<Insert **Table 2**>

2.2.7 Molecular modeling study of MAO-B. To further study the binding mode of **5b** and **5h** with MAO-B, molecular docking studies based on the X-ray crystal structures of human MAO-B (PDB code: 2V60) were performed [25]. In **5b**-MAO-B complex (**Figure 7A**), the hydroxyl group and carbonyl group of **5b** formed intramolecular hydrogen bonding interaction, and the hydroxyl group and the carbonyl group interacted with important amino acid Ile199 and Tyr326 via intermolecular hydrogen bonding, respectively. The O atom and the carbonyl of *O*-carbamate moiety could simultaneously interact with Tyr398 via intermolecular hydrogen bonding. In addition, the benzene ring of chalcone skeleton interacted with Cys172 via σ-π interaction. While, in the **5h**-MAO-B complex (**Figure 7B**), some characteristic interactions were observed, the carbonyl of *O*-carbamate moiety interacted with amine acid Tyr435 intermolecular hydrogen bonding. Moreover, the benzene ring of chalcone skeleton interacted with Ile199 forming σ-π interaction. Besides, some hydrophobic

interactions could be observed between the ligands (**5b** and **5h**) and MAO-B. Thus, the phenomenon observed might provide possible explanation that compounds **5b** and **5h** could decrease the MAO-B inhibitory activity.

<Insert **Figure 7**>

2.2.8 Inhibition of Self-induced Aβ_{1-42} Aggregation. The potent selective BChE inhibitors **5a**, **5b**, **5c**, **5h**, **5i**, **5j** and **5l** were selected to evaluate the inhibitory activity toward self-induced A$\beta_{\mathbf{1-42}}$ aggregation using thioflavin T (ThT) fluorescence assay [35]. Curcumin was used as reference compound, and the parent compound **3** was also tested as control purpose. According to the screening data in **Table 2**, the parent compound **3** (70.6%) showed more inhibitory activity toward self-induced A$\beta_{\mathbf{1-42}}$ aggregation than curcumin (43.1%). All the tested compounds displayed better inhibitory potency than curcumin, but indicated lower inhibition than compound **3**. In addition, the monosubstituted carbamate derivatives (**5a-5c**) exhibited better inhibition than the disubstituted carbamate compounds (**5h-5j**, **5l**). The possible reason was that the hydroxyl group served as important role in inhibition of self-induced A$\beta_{\mathbf{1-42}}$ aggregation. Moreover, the tertiary amine unit produced no obvious effect on self-induced A$\beta_{\mathbf{1-42}}$ aggregation inhibition.

*2.2.9 Metal-chelating properties of compounds **5b** and **5h**.* The chelation ability of compounds **5b** and **5h** was assessed by UV-visual spectrometry using biometals such as Cu^{2+}, Fe^{2+}, Zn^{2+} and Al^{3+} [28, 29]. The results were depicted in **Figure 8**. The electronic spectra of **5b** indicated a red shift (the peak at 359 nm shifted to 435 nm and 428 nm, respectively) after adding $CuCl_2$ and $AlCl_3$. While, compound **5b** was treated with $FeSO_4$ and $ZnCl_2$, respectively, the electronic spectra presented no obvious shift. The results revealed that compound **5b** was a selective metal chelator and could selectively chelate Cu^{2+} and Al^{3+}. In addition, the electronic spectra of **5h** showed no significant changes after adding $CuCl_2$, $AlCl_3$, $FeSO_4$ and $ZnCl_2$, suggesting little or no complex formation between **5h** with Cu^{2+}, Al^{3+}, Fe^{2+} or Zn^{2+}. The phenomenon observed exhibited that the 2'-hydroxyl and carbonyl group of the chalcone nucleus contributed to the chelation.

The above results showed that compound **5b** could chelate Cu^{2+} and Al^{3+}, which

have been promising therapeutic applications in AD patients. In addition, several studies had shown that Cu^{2+} significantly contributed to the formation of senile plaques and the complex Aβ_{1-42}-Cu^{2+} produced more reactive oxygen species. Thus, compound **5b** could selective chelate Cu^{2+} and could simultaneously stop the formation of amyloid plaques and relieved oxidative stress.

<Insert **Figure 8**>

The stoichiometry of the **5b**-Cu^{2+} complex was determined using the molar ratio method. The UV spectra were recorded and treated by numerical subtraction of $CuCl_2$ and **16d** at corresponding concentrations at 435nm. As shown in **Figure 9**, the absorbance linearly increased initially and then plateaued. The two straight lines intersected at a mole fraction of 0.97, indicating a 1:1 stoichiometry for the complex **5b**-Cu^{2+}.

<Insert **Figure 9**>

2.2.10 Effects on Cu^{2+}-induced Aβ_{1-42} aggregation. Compound **5b** was a selective metal chelator, and could chelate Cu^{2+} to form the **5b**-Cu^{2+} complex. So, thioflavin T (ThT) binding assay was performed to evaluate inhibition and disaggregation effect of **5b** on Cu^{2+}-induced Aβ_{1-42} aggregation [38, 39]. The data from **Table 2** showed that compound **5b** significantly inhibit Cu^{2+}-induced Aβ_{1-42} aggregation (78.3%), which was higher than positive compound curcumin (73.4%). Moreover, **5b** could decompose Cu^{2+}-induced Aβ_{1-42} aggregation with 83.1% disaggregation rate at 25 μM, and displayed better disaggregation than curcumin (58.2%).

To further complement the ThT binding assay, transmission electron microscopy (TEM) was used to observe the Aβ_{1-42} aggregation phenomenon. For inhibition assay, as shown in **Figure 10B,** the fresh Aβ_{1-42} had aggregated into amyloid fibrils after adding 25 μM Cu^{2+} during 24 h incubation, while the fresh Aβ_{1-42} was treated with **5b**, under the same experiments, small bulk aggregates were observed. It implied that compound **5b** could inhibit Cu^{2+}-induced Aβ_{1-42} aggregation. As for disaggregation assay, **Figure 10D** displayed that the well-defined Aβ_{1-42} fibrils obviously decreased after adding **5b** for another 24 incubation, suggesting that **5b** could decompose the structure of Cu^{2+}-mediated Aβ aggregation fibrils. Therefore, the TEM phenomenon

further supported the conclusion that **5b** could inhibit and disaggregate Cu^{2+}-induced A$\beta_{1\text{-}42}$ aggregation fibrils.

<Insert **Figure 10**>

2.2.11 Neuroprotective effects on H_2O_2-induced PC12 cell injury. Compounds **5b** and **5h** were selected to assess the neuroprotective effects against H_2O_2–induced PC12 cell injury using 3-(4,5-dimethylthiazol-2-yl)-2,5- diphenyltetrazolium (MTT) assays [29]. As shown in **Figure 11**, treatment with 100 μM H_2O_2, the cell viability sharply declined to 49.6 % ($p < 0.01$) compared with the untreated group. It meant that the model worked well. Under the same experiments condition, the cell viabilities increased to 78.3% and 63.2% after adding compounds **5b** and **5h**, respectively at 10.0 μM. While, when the concentration of **5b** and **5h** reduced to 1.0 μM, the cell viabilities were 62.9% and 53.7%, respectively. Therefore, the phenomenon displayed that compound **5b** showed potent neuroprotective effect by capturing the hydroxyl radical, generated by H_2O_2.

<Insert **Figure 11**>

2.2.12 In vitro blood−brain barrier permeation assay. The parallel artificial membrane permeation assay of the blood−brain barrier (PAMPA-BBB) was used to assess the BBB permeability of **5b** and **5h** [35, 40]. We selected 11 commercial drugs to validate the assay (**Table S1**), and a good linear correlation was produced through the experimental data versus the reported values, $P_e(\text{exp}) = 0.9163P_e(\text{bibl.}) - 0.2247$ ($R^2 = 0.9558$) **(Figure S1**). In view of the limit established by *Di et al*. we pointed out that compounds with permeability above 3.44×10^{-6} cm/s could cross the BBB (**Table S2**). According to the measured permeability (**Table 3**), both **5b** and **5h** could cross the BBB *in vitro*.

<Insert Table 3>

2.2.13 Theoretical evaluation of ADME properties. Molinspiration property program

was used to evaluate the druglike properties of **5b** and **5d**, the items including log *P*, topological polar surface area (TPSA), the number of hydrogen-bond acceptors, and the number of hydrogen-bond donors [41]. The data were listed in **Table 4**, both **5b** and **5d** complied with the Lipinski's rule of five, serving as a potent drug candidate.

<Insert **Table 4**>

2.2.14 In vivo assay. From the above results, compound **5b** was chosen to evaluate the effect *in vivo*. Primarily, Kunming mice were treated with **5b** at doses of 20, 100, and 500 mg/kg (n = 10 per group), mice were observed continuously for the first 4 h through 14 days and did not observe any abnormal behavior and mortality changes. Secondly, the Y-maze (three arms) test was performed to further assess whether **5b** could improve scopolamine-induced memory impairment [29, 42]. As shown in **Figure 12A**, the total arm entries indicated that there was no obvious difference between the untreated group, model group (scopolamine alone), **5b** (2.6, 7.8 and 23.4 mg/kg) group and Riva. (rivastigmine, 6 mg/kg) group, suggesting that compound **5b** and rivastigmine presented no effect on spontaneous alternation behavior. From the results in **Figure 12B**, treatment with scopolamine (3 mg/kg, *i.p.*) alone, the alternation obviously decreased to 45.6% ($p<0.01$) compared with the untreated group (72.1%). However, the spontaneous alternation behavior remarkably increased after treating with rivastigmine (6 mg/kg) ($p< 0.01$) or **5b** (2.6, 7.8 and 23.4 mg/kg; $p > 0.05$, $p < 0.01$, and $p < 0.05$, respectively). In addition, the medium dose (7.8 mg/kg, 65.1%) showed the highest alternation among the three dose groups and displayed similar potency compared with rivastigmine (6 mg/kg) (65.3%). The high dose group (23.4 mg/kg, 59.5%) of **5b** showed lower alternation than that of medium dose group (7.8 mg/kg, 65.1%), the reason might be that the high dose group (23.4 mg/kg) of **5b** showed some neurotoxicity and the medium dose would be the optimal dose. Therefore, the results indicated that compound **5b** could improve short-term working memory in mice.

<Insert **Figure 12**>

3. Conclusion

In summary, a series of chalcone-*O*-carbamate derivatives was designed using the multi-target-directed ligands strategy to discover multifunctional agents for the treatment of Alzheimer's disease (AD). All the target compounds were synthesized and evaluated by multiple biological activities including AChE/BChE inhibition, MAO-A/MAO-B inhibition, antioxidant activities, $A\beta_{1-42}$ aggregation inhibition, metal-chelating properties and neuroprotective effects against H_2O_2-induced PC12 cell injury. The results displayed that compounds **5b** and **5h** were considered as optimal multifunction agents, **5b** and **5h** were highly selective BChE inhibitors with IC_{50} values of 3.1 μM and 1.2 μM, respectively, and showed highly selective MAO-B inhibitory potency with IC_{50} values of 1.3 μM and 3.7 μM, respectively. In addition, compounds **5b** and **5h** could inhibit self-induced $A\beta_{1-42}$ aggregation with 63.9% and 53.1% inhibition, respectively. Furthermore, compounds **5b** and **5h** could cross the blood-brain barrier (BBB) *in vitro* and conformed to the Lipinski's rule of five. In particular, compound **5b** showed potent antioxidant activity (ORAC = 1.3 *eq*) and neuroprotective effect. Compound **5b** served as selective metal chelator by chelating Cu^{2+} and Al^{3+}, and could inhibit and disaggregate Cu^{2+}-induced $A\beta_{1-42}$ aggregation, which was further supported by the TEM images. Further, compound **5b** could improve scopolamine-induced cognitive impairment *in vivo* assay. Therefore, the results indicated that compound **5b** could be a promising multi-functional agent for the treatment of AD, and the further study and the structure optimization are in progress.

4. Experiment section

4.1. Chemistry. All materials were obtained from commercial suppliers. The reaction was monitored by thin-layer chromatography (TLC) on silica gel GF254 plates. The crude products were purified by column chromatography using silica gel (230-400 mesh), and the purity of compounds was determined by high-performance liquid chromatography (HPLC) analysis to be over 96%. HPLC analysis was carried out on a Shimadzu LC-10Avp plus system with the use of a Kromasil C_{18} column (4.6 mm × 250 mm, 5um). The ^{1}H NMR and ^{13}C NMR spectra of target compounds were recorded

using a Bruker 400 NMR spectrometer, and mass spectra were recorded on Agilent-6210 TOF LC-MS Spectrometer.

*4.1.1. The synthesis of intermediate **3**.* The starting material 2-hydroxy acetophenone **1** (1.0 mol) was treated with 3-hydroxybenzaldehyde **2** (1.0 mol) in the presence of an amount of a 30% aqueous KOH (4.0 mol) in in EtOH (25 mL) for 3 days, the reaction was monitored by TLC. After the reaction completed, the mixture was poured into ice-cold water. Acidified with 10% HCl, overnight, a yellow precipitate formed and filtrated, the residue was recrystallized with 80% ethanol to get golden yellow solid **3.** *(E)-3-(2-Hydroxyphenyl)-1-(3-hydroxyphenyl)prop-2-en-1-one (**3**).* Golden yellow solid, yield: 78.2%. ^{1}H NMR 12.78 (s, 1H, OH), 7.92 (d, *J* = 8.0 Hz, 1H, Ar-H), 7.86 (d, *J* = 15.6 Hz, 1H, CH=CH), 7.63 (d, *J* = 15.6 Hz, 1H, CH=CH), 7.51 (t, *J* = 8.0 Hz, 1H, Ar-H), 7.32 (t, *J* = 7.6 Hz, 1H, Ar-H), 7.25 (d, *J* = 9.2 Hz, 1H, Ar-H), 7.14 (s, 1H, Ar-H), 7.04 (d, *J* = 8.0 Hz, 1H, Ar-H), 6.95 (t, *J* = 8.0 Hz, 1H, Ar-H), 6.92 (d, *J* = 8.4 Hz, 1H, Ar-H), 5.06 (s, 1H, OH).

*4.1.2 General procedures for the synthesis of target compounds **5a-5f**.* To a mixture of intermediate 3 (1.0 mmol), anhydrous K_2CO_3 (1.2 mmol), and 4-DMAP (0.03 mmol) in 4 mL MeCN, *N,N*-disubstituted carbamoyl chlorides (**4a-f**) (1.1 mmol)was added dropwise at -5°C. The mixture was heated at 65°C for 6–8 h, the solvent was evaporated under reduced pressure. Water (25 ml) was added to the residue and the mixture was extracted with CH_2Cl_2 (2 × 25 mL). The combined organic phases were washed saturated aqueous sodium chloride (30 mL), dried over anhydrous Na_2SO_4, and filtered. The solvent was evaporated under a vacuum to give the crude product which was purified by column chromatography on silica gel (petroleum/acetone = 30: 1 as eluent) to get the desired products **5a-5f**.

*(E)-3-(3-(2-Hydroxyphenyl)-3-oxoprop-1-en-1-yl)phenyl dimethylcarbamate (**5a**).* Pale yellow oil, yield: 56.2%, 97.6% HPLC purity. ^{1}H NMR (400 MHz, $CDCl_3$) δ 12.78 (s, 1H, OH), 7.91 (d, *J* = 8.4 Hz, 1H, Ar-H), 7.87 (d, *J* = 16.0 Hz, 1H, CH=CH), 7.62 (d, *J* = 16.0 Hz, 1H, CH=CH), 7.52-7.46 (m, 3H, 3 × Ar-H), 7.42 (t, *J* = 7.6 Hz, 1H, Ar-H), 7.19 (t, *J* = 7.2 Hz, 1H, Ar-H), 7.03 (d, *J* = 8.0 Hz, 1H, Ar-H), 6.94 (t, *J* = 8.0 Hz, 1H, Ar-H), 3.09 (s, 3H, NCH_3), 3.00 (s, 3H, NCH_3). HR-ESI-MS: Calcd. For

$C_{18}H_{17}NO_4$ $[M + H]^+$: 312.1191, found: 312.1233.

*(E)-3-(3-(2-Hydroxyphenyl)-3-oxoprop-1-en-1-yl)phenyl ethyl(methyl)carbamate (**5b**).* Pale yellow oil, yield: 60.7%, 98.8% HPLC purity. ^{1}H NMR (400 MHz, $CDCl_3$) δ 12.79 (s, 1H, OH), 7.91 (d, *J* = 8.4 Hz, 1H, Ar-H), 7.88 (d, *J* = 15.6 Hz, 1H, CH=CH), 7.63 (d, *J* = 15.6 Hz, 1H, CH=CH), 7.51-7.45 (m, 3H, 3 × Ar-H), 7.41 (t, J = 8.0 Hz, 1H, Ar-H), 7.20 (t, *J* = 5.6 Hz, 1H, Ar-H), 7.02 (d, *J* = 8.4 Hz, 1H, Ar-H), 6.94 (t, *J* = 8.0 Hz, 1H, Ar-H), 3.50 (q, *J* = 7.2 Hz, 1H, 1/2 NCH_2), 3.43 (q, *J* = 7.2 Hz, 1H, 1/2 NCH_2), 3.10 (s, 3/2H, 1/2 NCH_3), 3.02 (s, 3/2H, 1/2 NCH_3), 1.27 (t, *J* = 6.8 Hz, 3/2 H, 1/2 CH_3), 1.21 (t, *J* = 7.2 Hz, 3/2 H, 1/2 CH_3). ^{13}C NMR 193.6, 163.6, 152.0, 144.6, 136.5, 136.0, 129.8, 129.7, 126.0, 124.4, 124.3, 121.3, 120.9, 120.0, 118.9, 118.6, 44.2, 34.3 (1/2 C), 33.9 (1/2 C), 13.3 (1/2 C), 12.5 (1/2 C). HR-ESI-MS: Calcd. For $C_{19}H_{19}NO_4$ $[M + H]^+$: 326.1348, found: 326.1379.

*(E)-3-(3-(2-Hydroxyphenyl)-3-oxoprop-1-en-1-yl)phenyl methoxy(methyl)carbamate (**5c**).* Pale yellow oil, yield: 36.5%, 97.4% HPLC purity. ^{1}H NMR (400 MHz, $CDCl_3$) δ 12.78 (s, 1H, OH), 7.91 (d, *J* = 8.0 Hz, 1H, Ar-H), 7.86 (d, *J* = 15.6 Hz, 1H, CH=CH), 7.62 (d, *J* = 15.6 Hz, 1H, CH=CH), 7.52-7.48 (m, 3H, 3 × Ar-H), 7.44 (t, *J* = 8.0 Hz, 1H, Ar-H), 7.19 (d, *J* = 7.6 Hz, 1H, Ar-H), 7.02 (d, *J* = 7.6 Hz, 1H, Ar-H), 6.94 (t, *J* = 8.0 Hz, 1H, Ar-H), 3.84 (s, 3H, OCH_3), 3.33 (s, 3H, NCH_3). HR-ESI-MS: Calcd. For $C_{18}H_{17}NO_5$ $[M + H]^+$: 328.1140, found: 328.1182.

*(E)-3-(3-(2-Hydroxyphenyl)-3-oxoprop-1-en-1-yl)phenyl diethylcarbamate (**5d**).* Pale yellow oil, yield: 50.9%, 98.6% HPLC purity. ^{1}H NMR (400 MHz, $CDCl_3$) δ 12.79 (s, 1H, OH), 7.93 (dd, J_1 = 6.8 Hz, J_2 = 1.2 Hz, 1H, Ar-H), 7.89 (d, *J* = 15.6 Hz, 1H, CH=CH), 7.65 (d, *J* = 15.6 Hz, 1H, CH=CH), 7.53-7.46 (m, 3H, 3 × Ar-H), 7.43 (t, *J* = 7.6 Hz, 1H, Ar-H), 7.21 (d, *J* = 8.0 Hz, 1H, Ar-H), 7.03 (d, *J* = 8.4 Hz, 1H, Ar-H), 6.95 (t, *J* = 8.0 Hz, 1H, Ar-H), 3.50-3.38 (m, 4H, 2 × NCH_2), 3.19-3.13 (m, 6H, 2 × CH_3). ^{13}C NMR 193.6, 163.6, 153.9, 152.1, 144.6, 136.5, 136.0, 129.8, 125.9, 124.3, 121.3, 120.9, 120.0, 118.9, 118.6, 42.4, 42.0, 14.3, 13.4. HR-ESI-MS: Calcd. For $C_{20}H_{21}NO_4$ $[M + H]^+$: 340.1504, found: 340.1549.

*(E)-3-(3-(2-Hydroxyphenyl)-3-oxoprop-1-en-1-yl)phenyl diphenylcarbamate (**5e**).* Pale yellow oil, yield: 42.3%, 97.3% HPLC purity. ^{1}H NMR (400 MHz, $CDCl_3$) δ

12.75 (s, 1H, OH), 7.91 (d, *J* = 8.0 Hz, 1H, Ar-H), 7.86 (d, *J* = 15.6 Hz, 1H, CH=CH), 7.62 (d, *J* = 15.2 Hz, 1H, CH=CH), 7.52-7.48 (m, 2H, 2 × Ar-H), 7.45-7.34 (m, 10H, 10 × Ar-H), 7.29-7.20 (m, 3H, 3 × Ar-H), 7.02 (d, *J* = 8.4 Hz, 1H, Ar-H), 6.94 (t, *J* = 7.6 Hz, 1H, Ar-H). ^{13}C NMR 193.6, 163.6, 155.7, 151.6, 149.0, 148.6, 144.4, 137.0, 136.5, 133.8, 131.5, 129.9, 129.8, 128.7, 126.9, 126.8, 126.3, 123.9, 121.1, 120.9, 120.8, 120.0, 118.9, 118.7, 110.8. HR-ESI-MS: Calcd. For $C_{28}H_{21}NO_4$ $[M + H]^+$: 436.1504, found: 436.1549

*(E)-3-(3-(2-Hydroxyphenyl)-3-oxoprop-1-en-1-yl)phenyl morpholine-4-carboxylate (**5f**).* Pale yellow oil, yield: 61.2%, 98.7% HPLC purity. ^{1}H NMR (400 MHz, $CDCl_3$) δ 12.72 (s, 1H, OH), 7.83 (d, *J* = 8.0 Hz, 1H, Ar-H), 7.80 (d, *J* = 16.0 Hz, 1H, CH=CH), 7.56 (d, *J* = 15.6 Hz, 1H, CH=CH), 7.42 (t, *J* = 8.4 Hz, 2H, 2 × Ar-H), 7.35 (t, *J* = 7.6 Hz, 2H, 2 × Ar-H), 7.12 (d, *J* = 8.0 Hz, 1H, Ar-H), 6.95 (d, *J* = 8.4 Hz, 1H, Ar-H), 6.86 (t, *J* = 7.6 Hz, 1H, Ar-H), 3.69-3.67 (m, 4H, 2 × NCH_2), 3.63-3.62 (m, 2H, OCH_2), 3.52-3.51 (m, 2H, OCH_2). ^{13}C NMR 193.5, 163.6, 153.4, 151.7, 144.4, 136.6, 136.0, 130.0, 129.8, 126.3, 124.3, 121.2, 120.9, 119.9, 119.0, 118.7, 66.7, 66.5, 44.9, 44.2. HR-ESI-MS: Calcd. For $C_{20}H_{19}NO_5$ $[M + H]^+$: 354.1297, found: 354.1346

*4.1.3 General procedures for the synthesis of target compounds **5g-5l.*** The detailed procedure referenced the To a mixture of intermediate 3 (1.0 mmol), anhydrous K_2CO_3 (3.0 mmol), and 4-DMAP (0.03 mmol) in 5 mL MeCN, The appropriate *N*,*N*-disubstituted carbamoyl chlorides (**4a-f**) (2.5 mmol) was added dropwise at -5°C. The mixture was heated at 65°C for 10-15 h, the solvent was treted according to synthesis of **5a-5l**. The target compounds 5g-5l were obtained using column chromatography on silica gel (petroleum/acetone = 50: 1 as eluent)

*(E)-3-(3-(2-((Dimethylcarbamoyl)oxy)phenyl)-3-oxoprop-1-en-1-yl)phenyl dimethylcarbamate (**5g**).* Pale yellow oil, yield: 30.2%, 98.7% HPLC purity. ^{1}H NMR (400 MHz, $CDCl_3$) δ 7.65 (dd, J_1 = 6.4 Hz, J_2 = 1.2 Hz, 1H, Ar-H), 7.54 (d, *J* = 16.0 Hz, 1H, CH=CH), 7.53-7.50 (m, 1H, Ar-H), 7.38 (d, *J* = 4.8 Hz, 2H, 2 × Ar-H), 7.33-7.30 (m, 2H, 2 × Ar-H), 7.22 (d, *J* = 8.0 Hz, 1H, Ar-H), 7.17-7.14 (m, 1H, Ar-H), 7.12 (d, *J* = 16.0Hz, 1H, CH=CH), 3.10 (s, 3H, NCH_3), 3.01 (s, 3H, NCH_3), 2.97 (s, 3H, NCH_3), 2.89 (s, 3H, NCH_3). ^{13}C NMR 192.2, 154.6, 154.2, 151.9, 149.4, 143.9,

135.9, 132.6, 132.4, 129.8, 129.6, 126.5, 125.5, 125.4, 124.1, 123.8, 121.2, 36.7, 36.6, 36.5, 36.4. HR-ESI-MS: Calcd. For $C_{21}H_{22}N_2O_5$ $[M + H]^+$: 383.1562, found: 383.1605

*(E)-3-(3-(2-((Ethyl(methyl)carbamoyl)oxy)phenyl)-3-oxoprop-1-en-1-yl)phenyl ethyl(methyl)carbamate (**5h**).* Pale yellow oil, yield: 35.1%, 97.7% HPLC purity. ^{1}H NMR (400 MHz, $CDCl_3$) δ 7.63 (t, *J* = 8.0 Hz, 1H, Ar-H), 7.54 (d, *J* = 14.8 Hz, 1H, CH=CH), 7.52-7.50 (m, 1H, Ar-H), 7.38 (d, *J* = 8.4 Hz, 2H, 2 × Ar-H), 7.31 (t, *J* = 6.4 Hz, 2H, 2 × Ar-H), 7.23 (t, *J* = 7.6 Hz, 1H, Ar-H), 7.17-7.15 (m, 1H, Ar-H), 7.11 (d, *J* = 16.0Hz, 1H, CH=CH), 3.48 (q, *J* = 7.2 Hz, 1H, 1/2 NCH_2), 3.41 (q, *J* = 7.2 Hz, 1H, 1/2 NCH_2), 3.36 (q, *J* = 7.2 Hz, 1H, 1/2 NCH_2), 3.30 (q, *J* = 7.2 Hz, 1H, 1/2 NCH_2), 3.08 (s, 3/2H, 1/2 NCH_3), 3.00 (s, 3/2H, 1/2 NCH_3), 2.96 (s, 3/2H, 1/2 NCH_3), 2.89 (s, 3/2H, 1/2 NCH_3), 1.25 (t, *J* = 6.8 Hz, 3/2 H, 1/2 CH_3), 1.20 (t, *J* = 6.8 Hz, 3/2 H, 1/2 CH_3), 1.12 (t, *J* = 6.8 Hz, 3/2 H, 1/2 CH_3), 1.05 (t, *J* = 6.8 Hz, 3/2 H, 1/2 CH_3). HR-ESI-MS: Calcd. For $C_{23}H_{26}N_2O_5$ $[M + H]^+$: 411.1875, found: 411.1909.

*(E)-3-(3-(2-((Methoxy(methyl)carbamoyl)oxy)phenyl)-3-oxoprop-1-en-1-yl)phenyl methoxy(methyl)carbamate (**5i**).* Pale yellow oil, yield: 40.9%, 97.3% HPLC purity. ^{1}H NMR (400 MHz, $CDCl_3$) δ 7.69 (d, *J* = 6.4 Hz, 1H, Ar-H), 7.57 (d, *J* = 15.6 Hz, 1H, CH=CH), 7.55 (dd, J_1 = 13.6 Hz, J_2 = 2.0 Hz, 1H, Ar-H), 7.42 (s, 1H, Ar-H), 7.40-7.36 (m, 2H, 2 × Ar-H), 7.34 (d, *J* = 6.8 Hz, 1H, Ar-H), 7.25 (d, *J* = 6.8 Hz, 1H, Ar-H), 7.22-7.20 (m, 1H, Ar-H), 7.18 (d, *J* = 16.0 Hz, 1H, CH=CH), 3.81 (s, 3H, OCH_3), 3.71 (s, 3H, OCH_3), 3.30 (s, 3H, NCH_3), 3.21 (s, 3H, NCH_3). ^{13}C NMR 193.2, 164.6, 161.8, 149.0, 144.1, 132.5, 129.9, 129.8, 126.5, 126.0, 125.9, 123.8, 123.6, 121.1, 35.6, 35.5, 29.7, 29.6. HR-ESI-MS: Calcd. For $C_{21}H_{22}N_2O_7$ $[M + H]^+$: 415.1461, found: 415.1510.

*(E)-3-(3-(2-((Diethylcarbamoyl)oxy)phenyl)-3-oxoprop-1-en-1-yl)phenyl diethylcarbamate (**5j**).* Pale yellow oil, yield: 40.9%, 97.3% HPLC purity. ^{1}H NMR (400 MHz, $CDCl_3$) δ 7.61 (d, *J* = 7.2 Hz, 1H, Ar-H), 7.54 (d, *J* = 16.0 Hz, 1H, CH=CH), 7.50-7.45 (m, 1H, Ar-H), 7.37-7.36 (m, 2H, 2 × Ar-H), 7.31-7.26 (m, 2H, 2 × Ar-H), 7.22 (d, *J* = 8.0 Hz, 1H, Ar-H), 7.16 (d, *J* = 3.6 Hz, 1H, Ar-H), 7.10 (d, *J* = 16.0Hz, 1H, CH=CH), 3.46-3.31 (m, 4H, 2 × NCH_2), 1.25-1.19 (m, 6H, 2 × CH_3).

HR-ESI-MS: Calcd. For $C_{25}H_{30}N_2O_5$ $[M + H]^+$: 439.2188, found: 439.2246.

*(E)-3-(3-(2-((Diphenylcarbamoyl)oxy)phenyl)-3-oxoprop-1-en-1-yl)phenyl diphenylcarbamate (**5k**).* Pale yellow oil, yield: 34.7%, 97.4% HPLC purity. ^{1}H NMR (400 MHz, $CDCl_3$) δ 7.59 (d, *J* = 7.6 Hz, 1H, Ar-H), 7.50 (d, *J* = 16.0 Hz, 1H, CH=CH), 7.46 (t, *J* = 7.6 Hz, 1H, Ar-H), 7.35-7.29 (m, 12H, 12 × Ar-H), 7.26-7.20 (m, 12H, 12 × Ar-H), 7.11 (t, *J* = 8.0 Hz, 2H, 2 × Ar-H), 7.03 (d, *J* = 16.0 Hz, 1H, CH=CH). ^{13}C NMR 192.8, 191.9 (2C), 152.8, 152.6, 151.6, 149.0, 144.1, 142.3, 142.2, 142.1, 136.1, 132.7, 132.3, 129.8, 129.7, 129.2 (6C), 129.1 (6C), 126.9, 126.8, 126.7 (2C), 126.6 (2C), 126.5, 125.9, 125.8, 123.8 (2C), 123.3, 121.2 (2C). HR-ESI-MS: Calcd. For $C_{41}H_{30}N_2O_6$ $[M + H]^+$: 631.2188, found: 631.2227.

*(E)-3-(3-(2-((Morpholine-4-carbonyl)oxy)phenyl)-3-oxoprop-1-en-1-yl)phenyl morpholine-4-carboxylate (**5l**).* Pale yellow oil, yield: 50.6%, 98.3% HPLC purity. ^{1}H NMR (400 MHz, $CDCl_3$) δ 7.57 (d, *J* = 7.6 Hz, 1H, Ar-H), 7.47 (d, *J* = 15.2 Hz, 1H, Ar-H), 7.44 (d, *J* = 16.8 Hz, 1H, CH=CH), 7.34-7.32 (m, 2H, 2 × Ar-H), 7.26 (t, *J* = 6.8 Hz, 2H, 2 × Ar-H), 7.15 (d, *J* = 8.4 Hz, 1H, Ar-H), 7.10-7.07 (m, 1H, Ar-H), 7.04 (d, *J* = 16.4 Hz, 1H, CH=CH), 3.69-3.65 (m, 4H, 2 × NCH_2), 3.61-3.58 (m, 2H, NCH_2), 3.51-3.48 (m, 8H, 4 × OCH_2), 3.38-3.36 (m, 2H, NCH_2). ^{13}C NMR 192.2, 153.3, 153.0, 151.7, 149.1, 144.3, 135.9, 132.4, 132.3, 130.0, 126.5, 125.8, 125.6, 124.0, 123.7, 121.4, 66.6, 66.5 (2C), 66.4, 44.9 (2C), 44.1 (2C). HR-ESI-MS: Calcd. For $C_{25}H_{26}N_2O_7$ $[M + H]^+$: 467.1774, found: 467.1821.

4.2 Biological evaluation

4.2.1 AChE and BuChE inhibition assay. The modified Ellman method was performed to test the AChE and BChE inhibitory ability of the compounds, using *ee*AChE and eqBChE (Sigma-Aldrich Co.). The detailed procedure referenced our previous work [28.31].

4.2.2. Antioxidant activity assay

The antioxidant activity was tested by the oxygen radical absorbance capacity f luorescein (ORAC-FL) assay. The details could reference our previous work [2 8, 29].

4.2.3. Recombinant human MAO-A and MAO-B inhibition studies. Recombinant

human MAO-A and MAO-B were purchased from Sigma-Aldrich and stored at -80 °C [36]. Solutions of test compounds were prepared in DMSO (2.5 mM) and diluted with potassium phosphate buffer (100 mM, pH 7.40, containing KCl 20.2 mM) to a final volume of 500 μL containing various concentrations of test compounds (0-100 μM) and kynuramine (45 μM for MAO-A and 30 μM for MAO-B). The reactions were initiated by the addition of the enzyme (7.5 μg/mL) and then incubated for 30 min at 37. Then 400 μL NaOH (2N) and 1000 μL water were added to terminated the enzymatic reactions and the mistures were centrifuged at 16000g for 10 min.[5] The concentrations of the MAOs generated 4-hydroxyquinoline were determined by measuring the fluorescence of the supernatant on a Varioskan Flash Multimode Reader (PerkinElmer) with excitation and emission wavelengths at 310 nm and 400 nm, respectively. A linear calibration curve was constructed by preparing samples containing 4-hydroxyquinoline (0.047–1.56 μM) dissolved in 500 μL potassium phosphate buffer. To each calibration standard, 400 μL NaOH (2 N) and 1000 μL water were added. The appropriate control samples were included to confirm that the test compounds do not fluoresce or quench the fluorescence of 4-hydroxyquinoline under the assay conditions. IC_{50} values were calculated from sigmoidal dose-response curves (graphs of the initial rate of kynuramine oxidation versus the logarithm of inhibitor concentration). Each sigmoidal curve was constructed form six different compound concentrations spanning at least three orders of magnitude. Data analyses were performed with GraphRad Prism 5 employing the one site competition model. IC_{50} values were determined in triplicate and expressed as mean ± SD.

4.2.4 Molecular docking. The crystal structure of BChE (PDB code: 4tpk), ACh E (PDB code: 1EVE) and MAO-B (PDB code: 2V60) were obtained from the Protein Data Bank after eliminating the original inhibitors and water molecules. [30] Docking studies were performed using the AUTODOCK 4.2 program. Gr aphic manipulations and visualizations were done by Autodock Tools or Discov ery Studio 2.5 software.

4.2.5. Metal binding studies. The metal binding studies were carried out in a Varioskan Flash Multimode Reader (Thermo Scientific) [28, 29]. The UV absorption of the tested compounds **5b** and **5h**, in the absence or presence of $CuCl_2$, $ZnCl_2$, $AlCl_3$ and $FeSO_4$ was recorded with wavelength ranging from 200 to 600 nm after incubating for 30 min in methanol at room temperature. The final volume of reaction mixture was 200 μL, and the final concentrations of tested compound and metals were 37.5 μM. The stoichiometry of the compound-Cu^{2+} complex was determined by titrating the methanol solution of tested compound with ascending of $CuCl_2$. The final concentration of tested compound was 37.5 μM, and the final concentration of Cu^{2+} ranged from 3.75 to 93.75 μM. The UV spectra were recorded and treated by numerical subtraction of $CuCl_2$ and tested compound at corresponding concentrations, plotted versus the mole fraction of tested compound.

4.2.6. Effect of test compounds on metal-induced Aβ_{1-42} aggregation experiments and disaggregation by ThT method. For the inhibition of Cu^{2+}-induced Aβ_{1-42} aggregation experiment [30, 38]. HEPES buffer solutions (20 mM, pH 6.6) containing 150 μM NaCl were prepared with distilled water. Solutions of Cu^{2+} were prepared from standards to concentration of 75 μM using the HEPES buffer at pH = 6.6. The Aβ_{1-42} stock solution was diluted in HEPES buffer. The mixture of the peptide (20 μL, 25 μM, final concentration) and Cu^{2+} (20 μL, 25 μM, final concentration), was incubated at 37 °C for 24h with or without the tested compound at different concentrations (20 μL, 25 μM, final concentration). After incubated, 190 μL of 5 μM Thioflavin T in 50 mM glycine-NaOH buffer (pH 8.5) was added. Each assay was run in triplicate. The detection method was the same as that of self-induced Aβ_{1-42} experiment.

For the disaggregation of copper-induced Aβ fibrils experiment, the Aβ_{1-42} stock solution was diluted in HEPES buffer (20 mM, pH 6.6, 150 mM NaCl). The mixture of the Aβ_{1-42} (20 μL, 25 μM, final concentration) with Cu^{2+} (20 μL, 25 μM, final concentration) was incubated 37 °C for 24 h. The tested compound (20 μL, 25 μM, final concentration) was then added and incubated at 37 °C for another 24 h. To minimize evaporation effect the wells were sealed by a transparent heat-resistant plastic film. After incubation, 190 μL of 5 μM thioflavin T in 50 mM glycine-NaOH

buffer (pH 8.5) was added. Each assay was run in triplicate. The detection method was the same as above.

4.2.7. Transmission Electron Microscopy (TEM) Assay. The preparation of samples could reference the self-induced and Cu^{2+}-induced A$\beta_{1\text{-}42}$ aggregation experiments. Aliquots (10 μL) of the samples were placed on a carbon-coated copper/rhodium grid for 2 min at room temperature. Excess sample was removed using filter paper followed by washing twice with ddH_2O. Each grid was incubated with uranyl acetate (1% w/v ddH_2O). Upon removal of excess uranyl acetate, the grids were dried for 15 min at room temperature. Images from each sample were taken on a Field Emission Transmission Electron Microscope (JEM-2100F).

4.2.8. In vitro blood−brain barrier permeation assay. The blood-brain barrier penetration of compounds was evaluated using the parallel artificial membrane permeation assay (PAMPA) described by Di *et al* [40]. Commercial drugs were purchased from Sigma and Alfa Aesar. Porcine brain lipid (PBL) was obtained from Avanti Polar Lipids. The donor microplate (PVDF membrane, pore size 0.45 mm) and acceptor microplate were both from Millipore. The 96-well UV plate (COSTAR) was from Corning Incorporated. The acceptor 96-well microplate was filled with 350 μL of PBS/EtOH (70:30), and the filter membrane was impregnated with 4 μL of PBL in dodecane (20 mg/mL). Compounds were dissolved in DMSO at 5 mg/mL and diluted 50-fold in PBS/EtOH (70:30) to a final concentration of 100 μg/mL. The detailed procedure refers to our previous work.

4.2.9. The Y–maze task. Rivastigmine was purchased from Shanghai Titan Technology Co., Ltd. Eisai China Inc. Scopolamine was purchase from J&K Scientific. Kunming mice at body weight of 18–22 g (six weeks old, either gender) were supplied by the Center of Experimental Animals of Sichuan Academy of Chinese Medicine Sciences (eligibility certification no. SCXK-Sichuan 2015-030). Mice were maintained under standard conditions with a 12 h:12 h light–dark cycle, a temperature and humidity controlled environment with access to food and water ad libitum..

The Y-maze test was performed to assess learning and memory in mice as previously described [29, 42]. Sixty mice were random divide into six groups. They

were *i.g.* compound **5b** (2.6 mg/kg, 7.8 mg/kg and 23.4 mg/kg), rivastigmine (6 mg/kg, as a positive control), same volume of water (untreated group or or model group) once respectively. After 30 min, memory impairment was induced by administering scopolamine (3 mg/kg, *i.p.*) or the same volume of normal saline (untreated group). Then 30 min later, the learning and memory capacitys of mouse were measured by the Y-maze test. The maze was made of black-colored acryl and positioned at equal angles. Rats were placed at the end of the arm and allowed to move freely through the maze during 8 min sessions. Arm entry sessions were recorded when the hind paws of the rat were completely placed in the arm. Consecutive entry into three arms in alternative order was defined as successive entries on overlapping triplet sets and the alternation percentage was calculated as the ratio of actual to possible alternations (defined as the total number of arm entries minus 2), multiplied by 100.

All data are expressed as mean ± SEM. Differences between groups were examined for statistical significance using one-way ANOVA with Student's *t* test. A *P* value less than 0.05 denoted the presence of a statistically significant difference.

AUTHOR INFORMATION

Corresponding Author

***** For Zhipei Sang: E-mail: sangzhipei@126.com

***** For Wenmin Liu: E-mail: liuwm1969@163.com

***** For Zhenghuai Tan: E-mail: tanzhh616@163.com

Author Contributions

The manuscript was written through contributions of all authors. All authors have given approval to the final version of the manuscript. #These authors contributed equally.

Notes

The authors declare no competing financial interest.

ACKNOWLEDGMENTS

This work was supported in part by the Foundation and Frontier Projects of Nanyang Science and Technology Bureau (2017JCQY020 and 2017 JCQY021)，the Special Project of Nanyang Normal University (SYKF2018081 and STP2018004).

Supporting Information Available:

The Tables and Figures in PAMPA-BBB experiments. The representative ^{1}H, ^{13}C NMR and HR-MS spectra for the synthesized compounds are available as supplementary material.

References

1. Barnett R. Alzheimer’s disease. Lancet. 2019, 393 (10181): 1589.
2. Marešová P, Mohelská H, Dolejš J, Kuča K. Socio-economic aspects of Alzheimer’s disease. Curr Alzheimer Res. 2015, 12(9): 903-911.
3. Lane CA, Hardy J, Schott JM. Alzheimer’s disease. Eur J Neurol. 2018, 25(1): 59-70.
4. Graham WV, Bonito-Oliva A, Sakmar TP. Update on Alzheimer’s disease therapy and prevention strategies. Annu Rev Med. 2017, 68: 413-430.
5. de Freitas Silva, M.; Dias, K.S.T.; Gontijo, V.S.; Ortiz, C.J.C.; Viega, C. Multi-target directed drugs as a modern approach for drug design towards Alzheimer's disease: an update. *Curr Med Chem.* **2018**, 25(29): 3491-3525.
6. Umar, T.; Hoda, N. Alzheimer's disease: A systemic review of substantial therapeutic targets and the leading multi-functional molecules. Curr Top Med Chem. 2017, 17(31): 3370-3389.
7. Ibrahim MM, Gabr MT. Multitarget therapeutic strategies for Alzheimer's disease. Neural Regen Res. 2019, 14(3): 437-440.
8. Li Q, He S, Chen Y, Feng F, Qu W, Sun H. Donepezil-based multi-functional cholinesterase inhibitors for treatment of Alzheimer's disease. Eur J Med Chem, 2018, 158:463-477.
9. Sameem B, Saeedi M, Mahdavi M, Shafiee A. A review on tacrine-based scaffolds as multi-target drugs (MTDLs) for Alzheimer's disease. Eur J Med

Chem. 2017, 128:332-345.

10. McHardy SF, Wang HL, McCowen SV, Valdez MC. Recent advances in acetylcholinesterase Inhibitors and Reactivators: an update on the patent literature (2012-2015). Expert Opin Ther Pat. 2017, 27(4):455-476.
11. Namdaung U, Athipornchai A, Khammee T, Kuno M, Suksamrarn S. 2-Arylbenzofurans from Artocarpus lakoocha and methyl ether analogs with potent cholinesterase inhibitory activity. Eur J Med Chem. 2018, 143: 1301-1311.
12. Furukawa-Hibi Y, Alkam T, Nitta A, Matsuyama A, Mizoguchi H, Suzuki K, Moussaoui S, Yu QS, Greig NH, Nagai T, Yamada K. Butyrylcholinesterase inhibitors ameliorate cognitive dysfunction induced by amyloid-β peptide in mice. Behav Brain Res. 2011, 225(1): 222-229.
13. Greig NH, Utsuki T, Ingram DK, Wang Y, Pepeu G, Scali C, Yu QS, Mamczarz J, Holloway HW, Giordano T, Chen D, Furukawa K, Sambamurti K, Brossi A, Lahiri DK. Selective butyrylcholinesterase inhibition elevates brain acetylcholine, augments learning and lowers Alzheimer beta-amyloid peptide in rodent. Proc Natl Acad Sci U S A. 2005, 102(47): 17213-17218.
14. Paroni G, Bisceglia P, Seripa D. Understanding the amyloid hypothesis in Alzheimer's disease. J Alzheimers Dis. 2019, 68(2): 493-510.
15. Ricciarelli R, Fedele E. The amyloid cascade hypothesis in Alzheimer’s disease: it’s time to change our mind. Curr Neuropharmacol. 2017, 15(6): 926-935.
16. Bonda DJ, Wang X, Perry G, Nunomura A, Tabaton M, Zhu X, Smith MA. Oxidative stress in Alzheimer disease: a possibility for prevention. Neuropharmacology. 2010, 59(4-5):290-294.
17. Butterfield DA, Halliwell B. Oxidative stress, dysfunctional glucose metabolism and Alzheimer disease. Nat Rev Neurosci. 2019, 20(3):148-160.
18. Cheignon C, Tomas M, Bonnefont-Rousselot D, Faller P, Hureau C, Collin F. Oxidative stress and the amyloid beta peptide in Alzheimer’s disease. Redox Biol. 2018, 14: 450-464.
19. Spinello A, Bonsignore R, Barone G, Keppler BK, Terenzi A. Metal ions and metal complexes in Alzheimer’s disease. Curr Pharm Des. 2016, 22(26):

3996-4010.

20. Drew SC. The case for abandoning therapeutic chelation of copper ions in Alzheimer's disease. Front Neurosci. 2017,11:317.
21. Kumar B, Gupta VP, Kumar V. A perspective on monoamine oxidase enzyme as drug target: challenges and opportunities. Curr Drug Targets. 2017, 18(1): 87-97.
22. Pazini AM, Gomes GM, Villarinho JG, da Cunha C, Pinheiro F, Ferreira AP, Mello CF, Ferreira J, Rubin MA. Selegiline reverses aβ_{25-35}-induced cognitive deficit in male mice. Neurochem Res. 2013, 38(11): 2287-2294.
23. Sano M, Ernesto C, Thomas RG, Klauber MR, Schafer K, Grundman M, Woodbury P, Growdon J, Cotman CW, Pfeiffer E, Schneider LS, Thal LJ. A controlled trial of selegiline, alpha-tocopherol, or both as treatment for Alzheimer's disease. The Alzheimer's Disease Cooperative Study. N Engl J Med. 1997, 336(17):1216-22.
24. Zhuang C, Zhang W, Sheng C, Zhang W, Xing C, Miao Z. Chalcone: a privileged structure in medicinal chemistry. Chem Rev 2017, 117(12): 7762-7810.
25. Zhang X, Rakesh KP, Bukhari SNA, Balakrishna M, Manukumar HM, Qin HL. Multi-targetable chalcone analogs to treat deadly Alzheimer's disease: Current view and upcoming advice. Bioorg Chem. 2018, 80: 86-93.
26. Kandiah N, Pai MC, Senanarong V, Looi I, Ampil E, Park KW, Karanam AK, Christopher S. Rivastigmine: the advantages of dual inhibition of acetylcholinesterase and butyrylcholinesterase and its role in subcortical vascular dementia and Parkinson's disease dementia. Clin Interv Aging. 2017, 12: 697-707.
27. Chaudhaery SS, Roy KK, Shakya N, Saxena G, Sammi SR, Nazir A, Nath C, Saxena AK. Novel carbamates as orally active acetylcholinesterase inhibitors found to improve scopolamine-induced cognition impairment: pharmacophore-based virtual screening, synthesis, and pharmacology. J Med Chem. 2010, 51(17): 6490-6505.
28. Sang Z, Qiang X, Li Y, Xu R, Cao Z, Song Q, Wang T, Zhang X, Liu H, Tan Z, Deng Y. Design, synthesis and evaluation of scutellarein-O-acetamidoalkylbenzylamines as potential multifunctional agents for

the treatment of Alzheimer's disease. Eur J Med Chem. 2017, 135: 307-323.

29. Sang Z, Li Y, Qiang X, Xiao G, Liu Q, Tan Z, Deng Y. Multifunctional scutellarin-rivastigmine hybrids with cholinergic, antioxidant, biometal chelating and neuroprotective properties for the treatment of Alzheimer's disease. Bioorg Med Chem. 2015, 23(4): 668-680.
30. Qiang X, Sang Z, Yuan W, Li Y, Liu Q, Bai P, Shi Y, Ang W, Tan Z, Deng Y. Design, synthesis and evaluation of genistein-O-alkylbenzylamines as potential multifunctional agents for the treatment of Alzheimer's disease. Eur J Med Chem. 2014, 76: 314-331.
31. Sang Z, Wang K, Han X, Cao M, Tan Z, Liu W. Design, synthesis, and evaluation of novel ferulic acid derivatives as multi-target-directed ligands for the treatment of Alzheimer's disease. ACS Chem Neurosci. 2019, 10(2):1008-1024.
32. Zarmouh, N.O.; Eyunni, S.K.; Soliman, K.F. The Benzopyrone Biochanin-A as a reversible, competitive, and selective monoamineoxidase B inhibitor. *BMC Complement Altern. Med*. **2017**, 17(1): 34.
33. Martini, F.; Bruning, C.A.; Soares, S.M.; Nogueira, C.W.; Zeni, G. Inhibitory effect of ebselen on cerebral acetylcholinesterase activity in vitro: kinetics and reversibility of inhibition. Curr. Pharm. Des. 2015, 21(7): 920-924.
34. Rosenberry, TL; Brazzolotto, X; Macdonald, IR; Wandhammer, M; Trovaslet-Leroy, M; Darvesh, S; Nachon, F. Comparison of the binding of reversible inhibitors to human butyrylcholinesterase and acetylcholinesterase: a crystallographic, kinetic and calorimetric study. Molecules. 2017, 22(12). Pii: E2098.
35. Sang, Z.; Pan, W.; Wang, K.; Ma, Q.; Yu, L.; Yang, Y.; Bai, P.; Leng, C.; Xu, Q.; Li, X.; Tan, Z.; Liu, W. Design, synthesis and evaluation of novel ferulic acid-O-alkylamine derivatives as potential multifunctional agents for the treatment of Alzheimer's disease. Eur. J. Med. Chem. 2017, 130, 379-392.
36. Li Y, Qiang X, Luo L, Yang X, Xiao G, Zheng Y, Cao Z, Sang Z, Su F, Deng Y. Multitarget drug design strategy against Alzheimer's disease: Homoisoflavonoid Mannich base derivatives serve as acetylcholinesterase and monoamine oxidase B

dual inhibitors with multifunctional properties. Bioorg Med Chem. 2017, 25(2): 714-726.

37. Bautista-Aguilera OM1, Samadi A, Chioua M, Nikolic K, Filipic S, Agbaba D, Soriano E, de Andrés L, Rodríguez-Franco MI, Alcaro S, Ramsay RR, Ortuso F, Yañez M, Marco-Contelles J.N-Methyl-N-((1-methyl-5-(3-(1-(2-methylbenzyl)piperidin-4-yl)propoxy)-1H-indol-2-yl)methyl)prop-2-yn-1-amine, a new cholinesterase and monoamine oxidase dual inhibitor. J Med Chem. 2014, 57(24): 10455-10463.
38. Sang Z, Qiang X, Li Y, Yuan W, Liu Q, Shi Y, Ang W, Luo Y, Tan Z, Deng Y. Design, synthesis and evaluation of scutellarein-O-alkylamines as multifunctional agents for the treatment of Alzheimer's disease. Eur J Med Chem. 2015, 94: 348-366.
39. Huang L, Lu C, Sun Y, Mao F, Luo Z, Su T, Jiang H, Shan W, Li X. Multitarget-directed benzylideneindanone derivatives: anti-β-amyloid (Aβ) aggregation, antioxidant, metal chelation, and monoamine oxidase B (MAO-B) inhibition properties against Alzheimer's disease. J Med Chem. 2012, 55(19): 8483-8492.
40. Di L, Kerns EH, Fan K, McConnell OJ, Carter GT. High throughput artificial membrane permeability assay for blood-brain barrier. Eur J Med Chem. 2003, 38(3): 223-232.
41. Matos MJ, Vilar S, Gonzalez-Franco RM, Uriarte E, Santana L, Friedman C, Tatonetti NP, Viña D, Fontenla JA. Novel (coumarin-3-yl)carbamates as selective MAO-B inhibitors: synthesis, in vitro and in vivo assays, theoretical evaluation of ADME properties and docking study. Eur J Med Chem. 2013, 63: 151-161.
42. Sun K, Bai Y, Zhao R, Guo Z, Su X, Li P, Yang P. Neuroprotective effects of matrine on scopolamine-induced amnesia via inhibition of AChE/BuChE and oxidative stress. Metab Brain Dis. 2019, 34(1):173-181.

Figures, Schemes and Tables

Figure 1. Design strategy of chalcone-*O*-carbamate derivatives

Figure 2 (A) *ee*AChE recovery after preincubation of compounds **5b** and **5h** diluted to 1× or 0.1 × IC_{50}, compared to standard rivastigmine and donepezil. (B)*ee*AChE recovey of rivastigmine, donepezil, compounds **5b** and **5h** diluted to 0.1 × IC_{50}, were monitored with time at room temperature. Data points, representing the average of three experiments, at least, were expressed as the mena ± SEM, n= 3.

Figure 3 Steady state inhibition by compound **5b** of the BChE hydrolysis of BCh.

Figure 4 (A) Representation of compound **5b** (green stick) interacting with residues in the binding site of BChE (PDB code: 4tpk). (B) 3D docking model of compound **5b** with BChE.

Figure 5 (A) **5h** (green stick) interacting with residues in the binding site of BChE (PDB code: 4tpk). (D) 3D docking model of **5h** with BChE.

Figure 6 (A) Representation of compound **5b** (green stick) interacting with residues in the binding site of *Tc*AChE (PDB code: 1EVE). (B) **5h** (green stick) interacting with residues in the binding site of *Tc*AChE.

Figure 7 Compounds (green stick) interacting with residues in the binding site of MAO-B (PDB code: 2V60), highlighting the protein residues that participate in the main interactions with the inhibitor. (A) 5b-MAO-B complex; (B) 5h-MAO-B complex.

Figure 8 The UV spectrum of compounds **5b** and **5h** (37.5 μM, in methanol) alone or in the presence of $CuCl_2$, $AlCl_3$, $ZnCl_2$ and $FeSO_4$ (37.5 μM, in methanol)

Figure 9 Determination of the stoichiometry of complex-Cu^{2+} by using molar ratio method through titrating the methanol solution of compound **5b** with ascending amounts of $CuCl_2$. The final concentration of tested compound was 37.5 μM.

Figure 10 (A) Scheme of the inhibition experiment; (B) TEM images of A*β* species from inhibition experiments. (C) Scheme of the disaggregation experiments; (D) TEM images of samples from disaggregation experiments.

Figure 11 Protective effects of **5b** and **5h** on cell injury induced by H_2O_2 (100 μM) in PC12 cells. $^{\#\#}p < 0.01$ *vs* control; $^{*}p < 0.05$ *vs* H_2O_2 group and $^{**}p < 0.01$ *vs* H_2O_2 group.

Figure 12 Effect of compound **5b** on scopolamine-induced cognitive impairment in the Y–maze test. (A) The total arm entries of the six groups of mice. (B) The percent of spontaneous alternation of mice. $^{\#\#}p < 0.01$ *vs* untreated group. $^{**}p < 0.01$ *vs* model group. $^{*}p < 0.05$ *vs* model group.

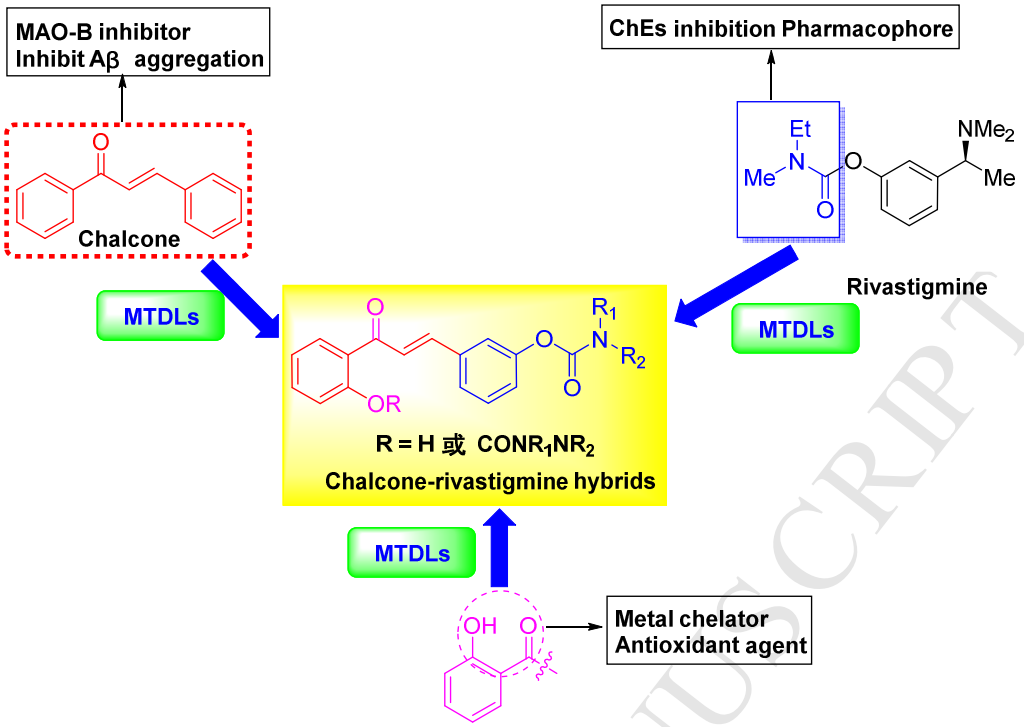

Figure 1. Design strategy of chalcone-*O*-carbamate derivatives

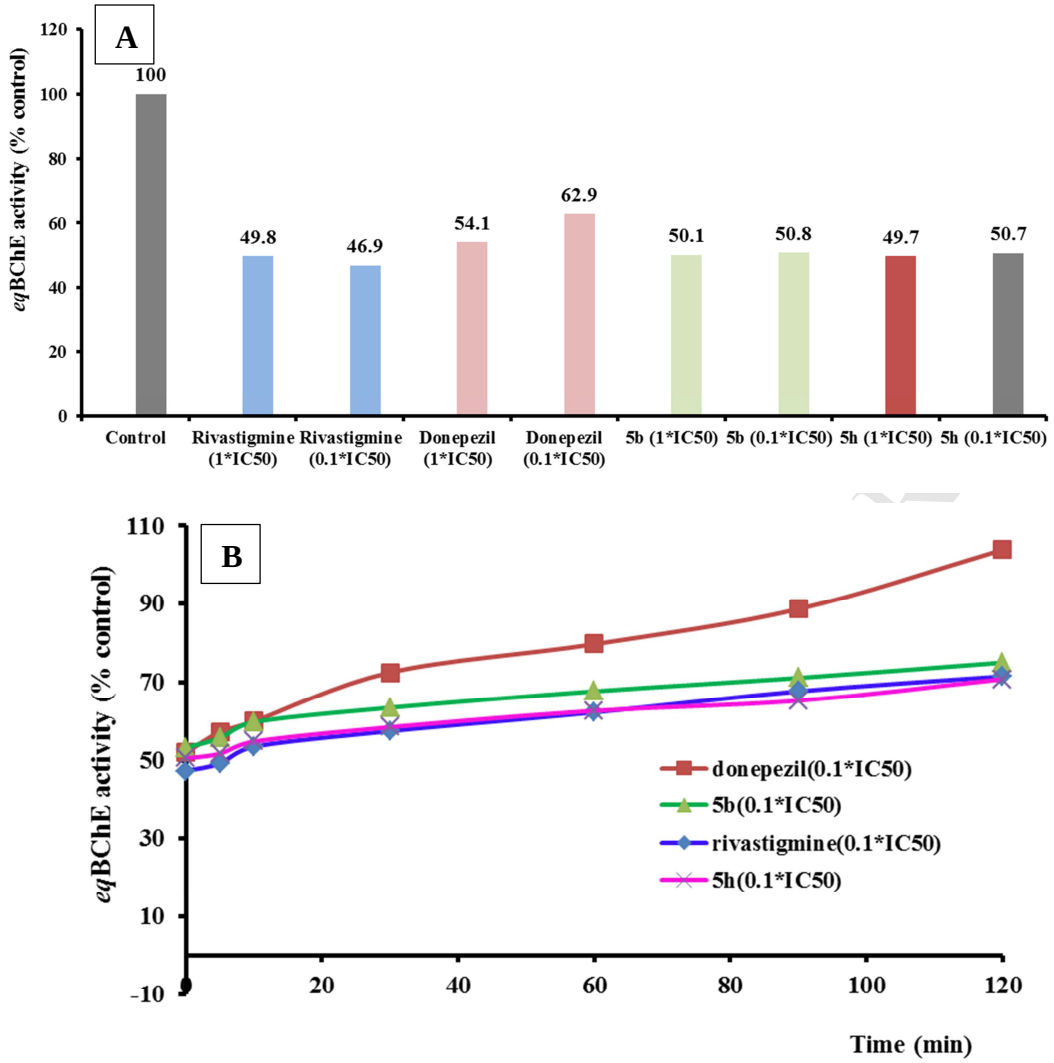

Figure 2 (A) *eqBChE* recovery after preincubation of compounds **5b** and **5h** diluted to 1× or 0.1 × IC_{50}, compared to standard rivastigmine and donepezil. (B) *eqBChE* recovey of rivastigmine, donepezil, compounds **5b** and **5h** diluted to 0.1 × IC_{50}, were monitored with time at room temperature. Data points, representing the average of three experiments, at least, were expressed as the mena±SEM, n= 3.

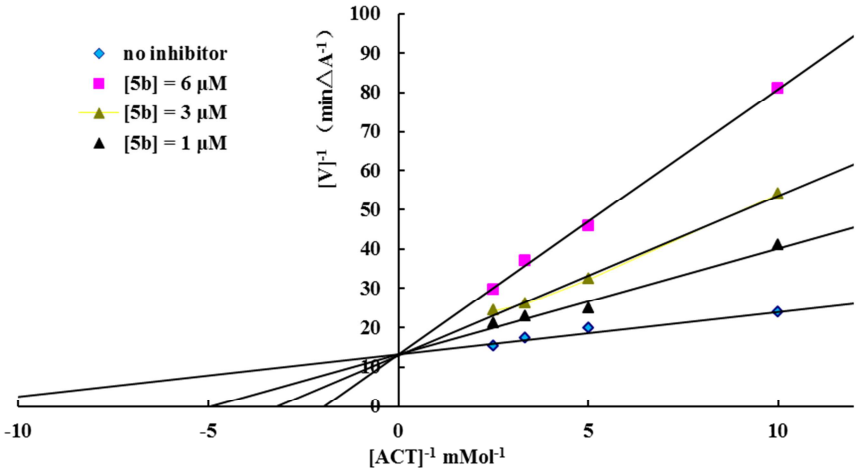

Figure 3 Steady state inhibition by compound **5b** of the BChE hydrolysis of BCh.

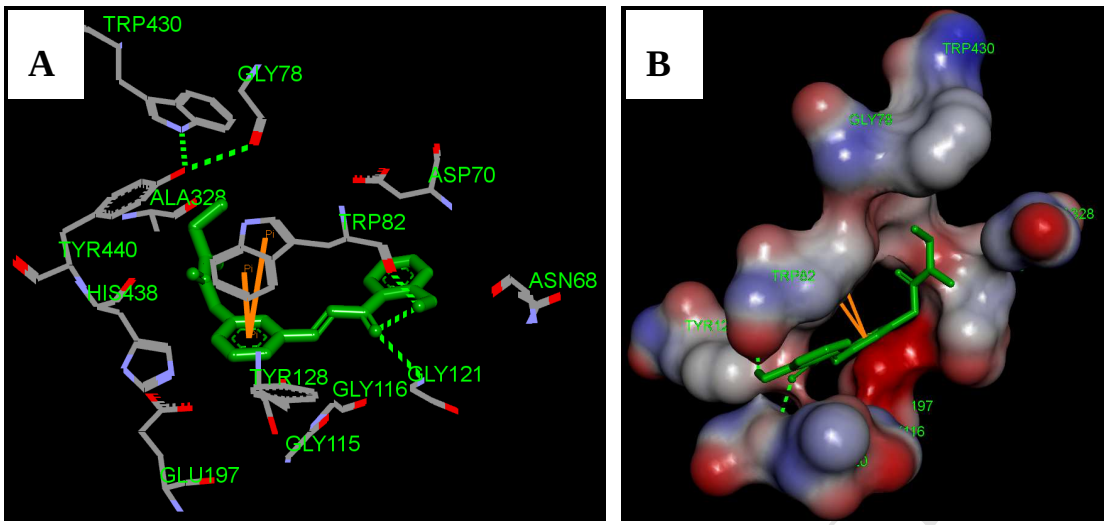

Figure 4 (A) Representation of compound **5b** (green stick) interacting with residues in the binding site of BChE (PDB code: 4tpk). (B) 3D docking model of compound **5b** with BChE.

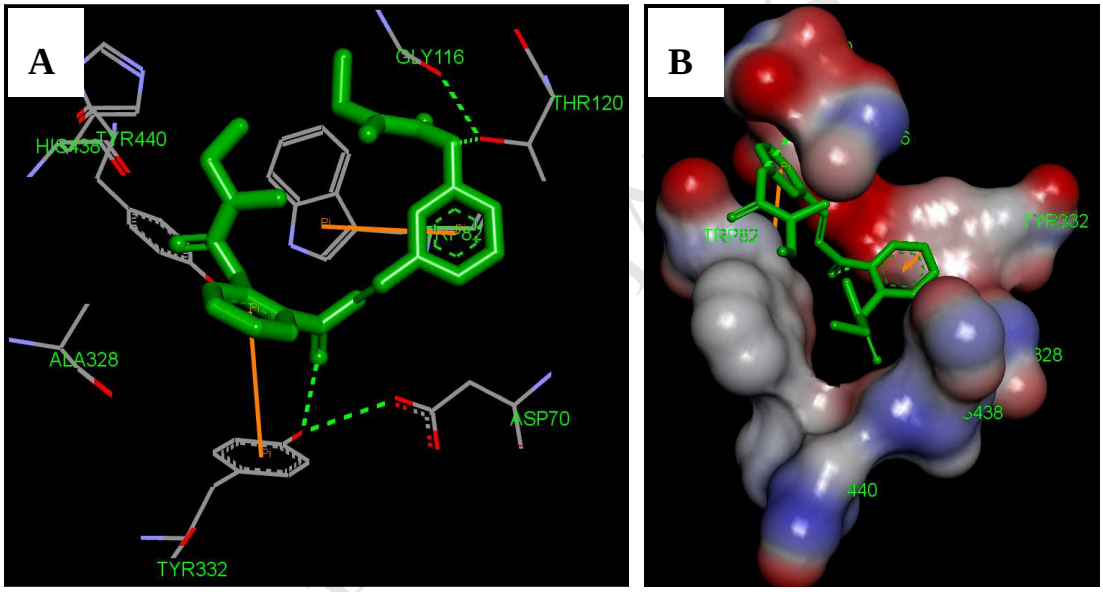

Figure 5 (A) **5h** (green stick) interacting with residues in the binding site of BChE (PDB code: 4tpk). (D) 3D docking model of **5h** with BChE.

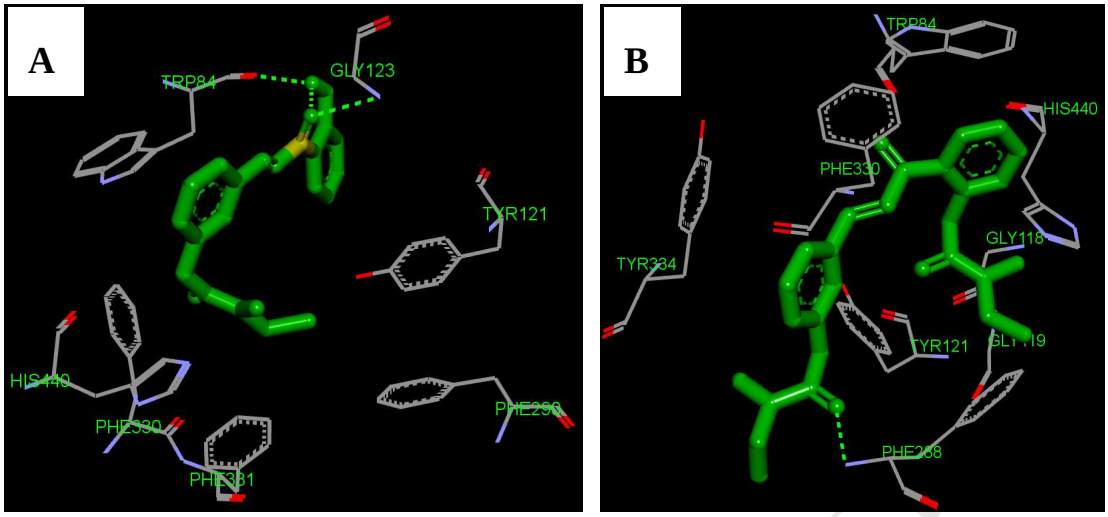

Figure 6 (A) Representation of compound **5b** (green stick) interacting with residues in the binding site of *Tc*AChE (PDB code: 1EVE). (B) **5h** (green stick) interacting with residues in the binding site of *Tc*AChE.

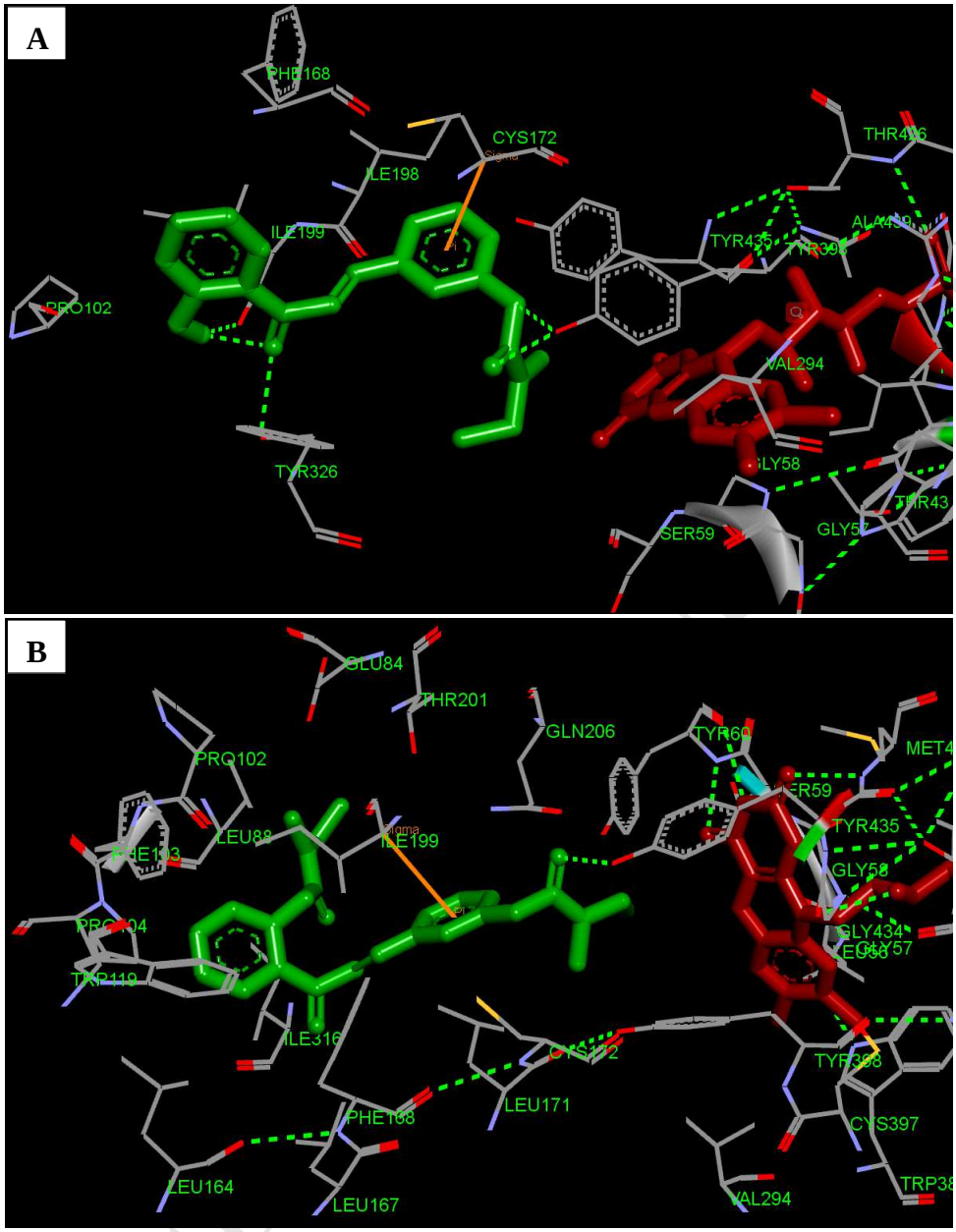

Figure 7 Compounds (green stick) interacting with residues in the binding site of MAO-B (PDB code: 2V60), highlighting the protein residues that participate in the main interactions with the inhibitor. (A) 5b-MAO-B complex; (B) 5h-MAO-B complex.

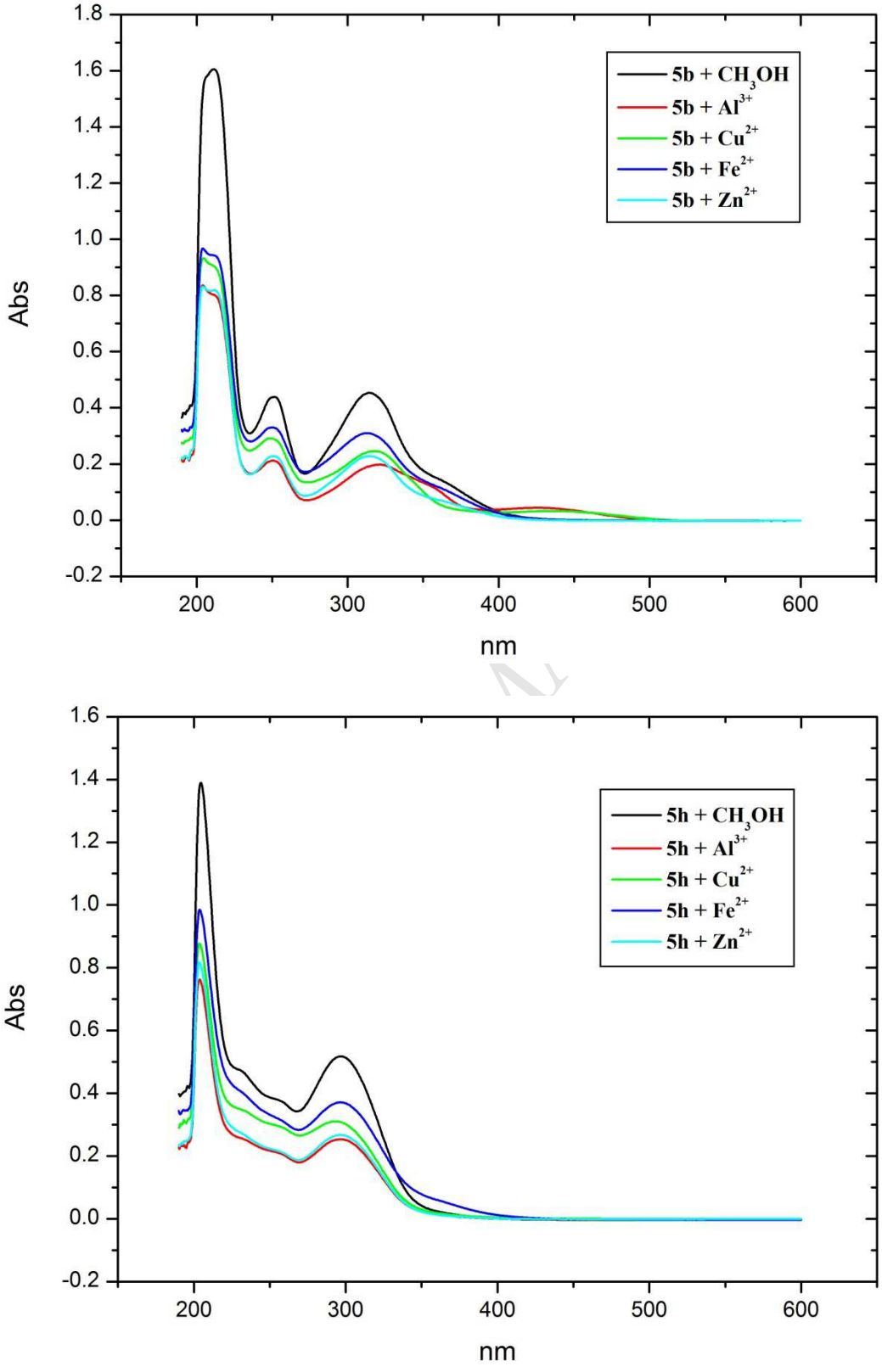

Figure 8 The UV spectrum of compounds **5b** and **5h** (37.5 μM, in methanol) alone or in the presence of $CuCl_2$, $AlCl_3$, $ZnCl_2$ and $FeSO_4$ (37.5 μM, in methanol)

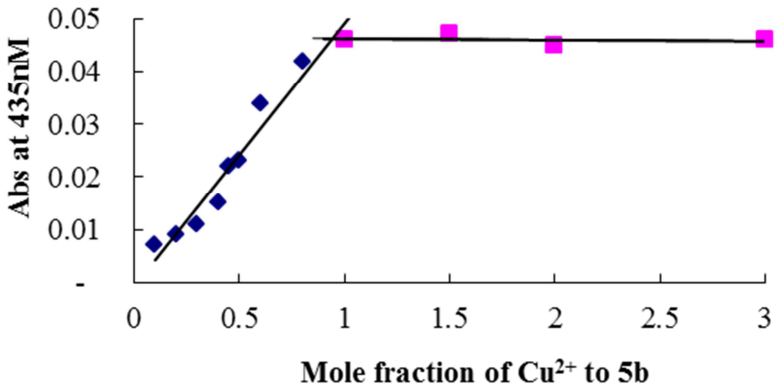

Figure 9 Determination of the stoichiometry of complex-Cu^{2+} by using molar ratio method through titrating the methanol solution of compound **5b** with ascending amounts of $CuCl_2$. The final concentration of tested compound was 37.5 μM.

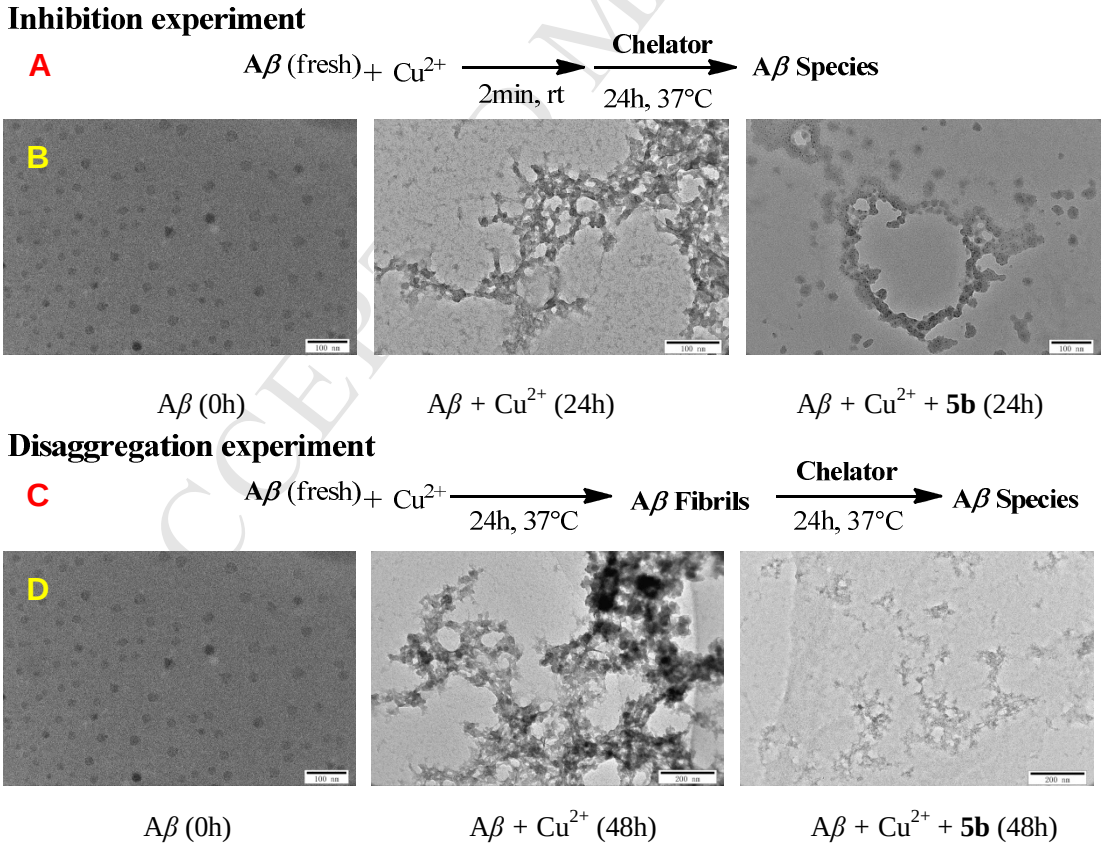

Figure 10 (A) Scheme of the inhibition experiment; (B) TEM images of Aβ species from inhibition experiments. (C) Scheme of the disaggregation experiments; (D) TEM images of samples from disaggregation experiments.

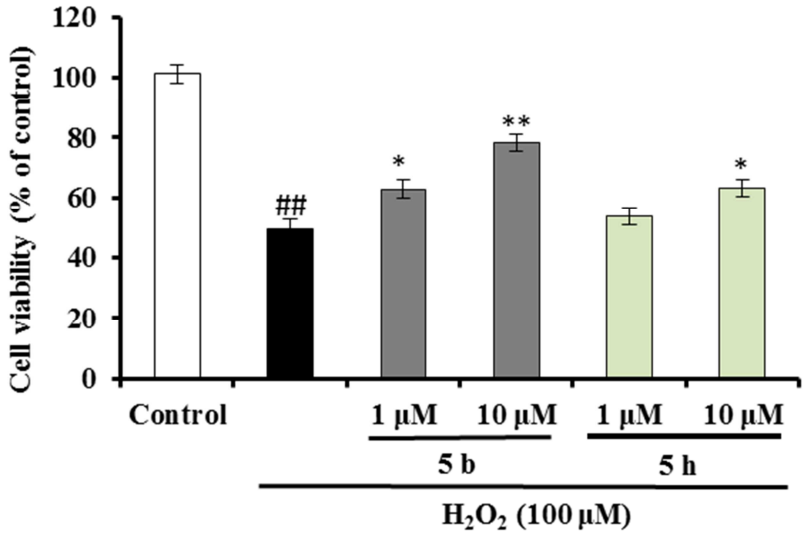

Figure 11 Protective effects of **5b** and **5h** on cell injury induced by H_2O_2 (100 μM) in PC12 cells. $^{\#\#}p < 0.01$ *vs* control; $^{*}p < 0.05$ *vs* H_2O_2 group and $^{**}p < 0.01$ *vs* H_2O_2 group.

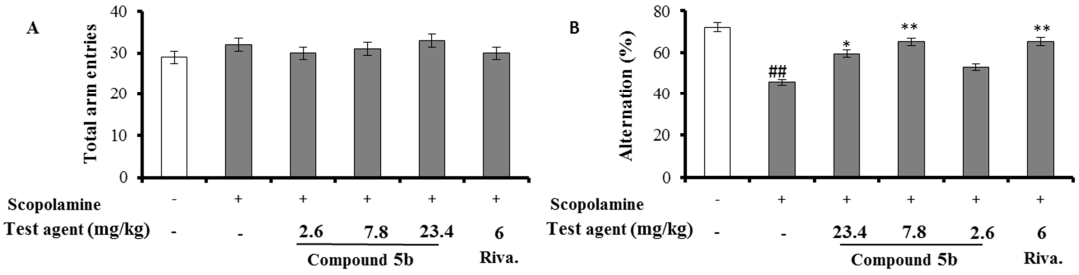

Figure 12 Effect of compound **5b** on scopolamine-induced cognitive impairment in the Y–maze test. (A) The total arm entries of the six groups of mice. (B) The percent of spontaneous alternation of mice. $^{\#\#}p < 0.01$ *vs* untreated group. $^{**}p < 0.01$ *vs* model group. $^{*}p < 0.05$ *vs* model group.

Scheme 1. The synthetic route of target compounds **5a-5l**. Reagents and conditions: (i) 50% aqueous KOH, EtOH, room temperature, 3 to 4 days. (ii) K_2CO_3, CH_3CN, 65℃, 6-15 h.

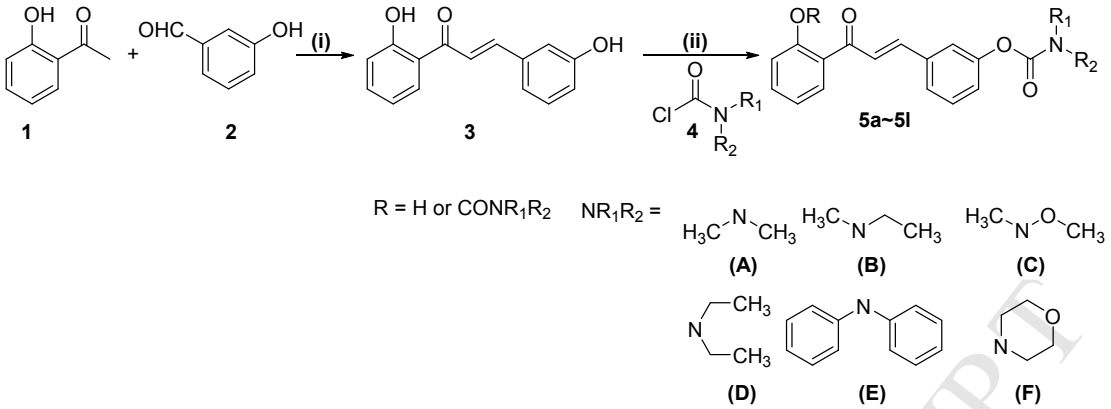

Scheme 1. The synthetic route of target compounds **5a-5l**. Reagents and conditions: (i) 50% aqueous KOH, EtOH, room temperature, 3 to 4 days. (ii) K_2CO_3, CH_3CN, 65℃, 6-15 h.

Table 1. AChE and BChE inhibitory activities and oxygen radical absorbance capacity (ORAC, Trolox equivalent) of chalcone-*O*-carbamate derivatives **5a-5l**, **3**, rivastigmine and donepezil.

Table 2. The MAO-B/MAO-A inhibition and effect on A$\beta_{1\text{-}42}$ aggregation of chalcone-*O*-carbamate derivatives and positive compounds.

Table 3. Permeability Pe ($\times 10^{-6}$ cm/s) in the PAMPA-BBB assay of the selected compounds **5b**, **5h** and their predictive penetration in the CNS.

Table 4. Theoretical prediction of the ADME properties of compounds **5b** and **5h**.

Table 1. AChE and BChE inhibitory activities and oxygen radical absorbance capacity (ORAC, Trolox equivalent) of chalcone-*O*-carbamate derivatives **5a-5l**, **3** and rivastigmine.

Compound	R	NR_1R_2	*ee*AChE [a]	*eq*BChE[b]	ORAC [e]
			(% inhibition) [c]	IC_{50} ± SD [d] (μM)	
5a	H	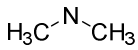	28.8±1.1%	2.51±0.05	1.1±0.03
5b	H	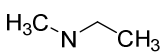	26.2±0.89%	3.1±0.02	1.3±0.02
5c	H	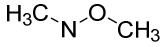	30.4±1.59%	3.2±0.03	1.2±0.04
5d	H		16.9±0.15%	4.8±0.02	1.3±0.03
5e	H	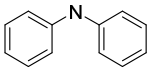	18.9±0.97%	56.2±2.8	1.1±0.05
5f	H		24.3±1.23%	5.1±0.41	1.2±0.02
5g	COR_1R_2	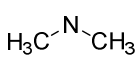	11.7±0.39%	4.5 ±0.06	0.32±0.02
5h	COR_1R_2	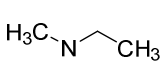	35.4±1.9%	1.2±0.05	0.35±0.02
5i	COR_1R_2	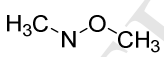	45.4±2.1%	1.5±0.03	0.32±0.01
5j	COR_1R_2		21.9±1.7%	3.1±0.25	0.31±0.02
5k	COR_1R_2	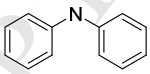	27.1±0.86%	42.6±2.5	0.33±0.01
5l	COR_1R_2		20.8±1.46%	2.0±0.01	0.32±0.02
3			23.3±2.33%	28.9±1.64% [c]	2.6±0.07
Rivastigmine			7.9±0.19μM [d]	1.3±0.05	N.T [f]
Donepezil			0.018±0.001μM [d]	4.76±0.02	N.T. [f]

[a] *ee*AChE from *electrophorus electricusc*. [b] *eq*BChE from *equine serum*. [c] % inhibition of *ee*AChE at a concentration of 25μM in the assay, data are the mean ± SEM of three independent experiments. [d] IC_{50} values represent the concentration of inhibitor required to decrease enzyme activity by 50% and are the mean of three independent experiments, values are expressed as the mean ± standard deviation of the mean of three independent experiments. [e] Results are expressed as μM of Trolox equivalent/μM of tested compounds. [f] NT = not tested.

Table 2. The MAO-B/MAO-A inhibition and effect on A$\beta_{1\text{-}42}$ aggregation of chalcone-*O*-carbamate derivatives and positive compounds.

Compound	IC_{50} (μM) ± SD [a]		Effect on of A$\beta_{1\text{-}42}$ aggregation (%)[e]		
	MAO-B [b]	MAO-A [c]	Inhibit self-induced [f]	Inhibit Cu^{2+}-induced [g]	Disaggregate Cu^{2+}-induced [h]
5a	0.8±0.01	19.9±0.87%[d]	60.2 ± 0.64	n.t. [i]	n.t. [i]
5b	1.3±0.06	16.4±0.32%[d]	63.9 ± 0.82	78.3 ± 2.7	83.1 ± 3.1
5c	2.6±0.03	33.8±0.79%[d]	61.4 ± 0.48	n.t. [i]	n.t. [i]
5d	1.8±0.02	38.1±1.8%[d]	n.t.	n.t. [i]	n.t. [i]
5e	4.9±0.05	18.2±0.67%[d]	n.t.	n.t. [i]	n.t. [i]
5f	3.1±0.08	17.4±1.7%[d]	n.t.	n.t. [i]	n.t. [i]
5g	2.9±0.02	18.9±1.3%[d]	n.t.	n.t. [i]	n.t. [i]
5h	3.7±0.04	28.4±0.56%[d]	53.1 ± 0.19	n.t. [i]	n.t. [i]
5i	4.6±0.02	10.3±0.29[d]	49.9 ± 0.52	n.t. [i]	n.t. [i]
5j	3.3±0.05	21.1±0.49%[d]	51.5 ± 0.43	n.t. [i]	n.t. [i]
5k	6.3± 0.01	18.2±1.1%[d]	n.t.	n.t. [i]	n.t. [i]
5l	5.2±0.03	20.9±0.38%[d]	49.2 ± 0.26	n.t. [i]	n.t. [i]
3	1.1± 0.03	28.1± 1.9%[d]	70.6 ± 0.34	n.t. [i]	n.t. [i]
Iproniazid	1.62 ± 0.06	5.59 ± 0.08	n.t. [i]	n.t. [i]	n.t. [i]
Rasagiline	0.031±0.002	0.62 ±0.03	n.t. [i]	n.t. [i]	n.t. [i]
Curcumin	n.t. [i]	n.t. [i]	45.7 ± 0.76	73.4 ± 1.2	58.2±2.6

[a] IC_{50} values represent the concentration of inhibitor required to decrease enzyme activity by 50% and are the mean of three independent experiments, each performed in triplicate (SD = standard deviation). [b] From recombinant human MAO-B. [c] From recombinant human MAO-A. [d] MAO-A percent inhibition rate of compounds at 12.5 μM. [e]Inhibition of A$\beta_{1\text{-}42}$ aggregation and disaggregation of A$\beta_{1\text{-}42}$ aggregation, the thioflavin-T fluorescence method was used, data are the mean ± SEM of three independent experiments. [f] Inhibition of self-Induced A$\beta_{1\text{-}42}$ aggregation, the concentration of tested compounds and A$\beta_{1\text{-}42}$ were 25 μM. [g] Inhibition of Cu^{2+}-induced A$\beta_{1\text{-}42}$ aggregation. The concentration of tested compounds and Cu^{2+} both were 25 μM. [h] Disaggregating of Cu^{2+}-induced A$\beta_{1\text{-}42}$ aggregation, the concentration of tested compounds and A$\beta_{1\text{-}42}$ were 25 μM. [i] n.t. = not tested.

Table 3. Permeability Pe ($\times 10^{-6}$ cm/s) in the PAMPA-BBB assay of the selected compounds **5b**, **5h** and their predictive penetration in the CNS.

compound[a]	Pe ($\times 10^{-6}$ cm/s)[b]	prediction
5b	15.67 ± 0.81	CNS+
5h	23.14 ± 1.12	CNS+

[a] Compound **5b** and **5h** was dissolved in DMSO at 5 mg/mL and diluted with PBS/EtOH (70:30). The final concentration of compounds was 100 μg/mL.

[b] Values are expressed as the mean ± SD of three independent experiments.

Table 4. Theoretical prediction of the ADME properties of compounds **5b** and **5h**.

Comp.	Log *P*	MW	TPSA (Å^2)	n-ON	n-OHNH	volume (Å^3)
5b	3.73	325.36	66.84	5	1	300.55
5h	3.74	410.47	76.16	7	0	383.20

[a] MW, Molecular weight; TPSA, topological polar surface area; n-OH, number of hydrogen acceptors; n-OHNH, number of hydrogen bond donors. The data was determined with the Molinspiration calculation software.

Highlights

- Compound **5b** was a reversible competition BChE inhibitor (IC_{50} = 3.1 μM) and selective MAO-B inhibitor (IC_{50} = 1.3 μM)
- Compound **5b** showed good antioxidant activity and neuroprotective effect.
- Compound **5b** was a selective metal chelator, and could significantly inhibit and decompose Cu^{2+}-induced $A\beta_{1-42}$ aggregation.
- Compound **5b** could cross PAMPA-BBB and conformed to the Lipinski's rule.
- Compound **5b** could improve scopolamine-induced memory impairment